Jürgen Novak, BSc

The role of α/β-hydrolase domain containing protein 15 (ABHD15) in brown adipose tissue

MASTER'S THESIS

to achieve the university degree of

Diplom-Ingenieur

Master's degree programme: Biomedical Engineering

submitted to

Graz University of Technology

Supervisor

Melina Amor PhD

Institute for Biochemistry

Graz, August 2018

EIDESSTATTLICHE ERKLÄRUNG

AFFIDAVIT

Ich erkläre an Eides statt, dass ich die vorliegende Arbeit selbstständig verfasst, andere als die angegebenen Quellen/Hilfsmittel nicht benutzt, und die den benutzten Quellen wörtlich und inhaltlich entnommenen Stellen als solche kenntlich gemacht habe. Das ins TUGRAZonline hochgeladene Textdokument ist mit der vorliegenden Masterarbeit identisch.

I declare that I have authored this thesis independently, that I have not used other than the declared sources/resources, and that I have explicitly indicated all material which has been quoted either literally or by content from the sources used. The text document uploaded to TUGRAZonline is identical to the present master's thesis.

Graz, 27.08.2018

Datum / Date

Unterschrift / Signature

Abstract

Overweight and obesity became an increasing worldwide problem. A sedentary lifestyle and excess of food led to an increase morbidity of non-communicable diseases. Hence, research focused with growing interest on the physiology of adipose tissue (AT). Mammals possess at least two types of AT, which can be distinguished into white adipose tissue (WAT) as storage organ and energy provider and brown adipose tissue (BAT) that dissipates energy to generate heat. This thesis intended to investigate the role of α/ß hydrolase domain containing protein 15 (ABHD15) in BAT and brown adipocytes. Studies have so far concentrated on the role of ABHD15 in WAT or white adipocytes. The aims of this thesis were to: 1) elucidate potential effects of constitutively Abhd15-knockout at the single gene and pathway levels in BAT, 2) investigate the role of ABHD15 in immortalized brown adipocytes during proliferation and differentiation, and 3) analyze the regulation of ABHD15 in murine BAT upon different nutritional status or cold exposure.

The first part of this thesis comprises results from microarray experiments and gene set enrichment analysis. I was able to identify an interesting pool of dysregulated genes and biological processes in BAT from Abhd15-knockout mice. These results indicate a potential influence of Abhd15 in a variety of biological processes such as energy homeostasis, reactive oxygen species production, and hormone metabolism. Additionally, I aimed to investigate the metabolic phenotype of an immortalized brown adipocyte cell line stably overexpressing *Abhd15* by proliferation and differentiation experiments. However, due to an observed differentiation defect, further investigations were not possible. Finally, I studied the effects of cold exposure, dietary composition, and fasting and refeeding on ABHD15 in BAT depots. Recent studies in WAT revealed that ABHD15 stabilizes phosphodiesterase 3B (PDE3B) and influences its expression. Mice with deletion of ABHD15 in WAT showed a reduced expression of PDE3B and induced an unrestrained fatty acid mobilization, accompanied by a reduced glucose uptake, which promotes insulin resistance. I could show in this thesis that PDE3B levels were also decreased in BAT from Abhd15-KO mice compared to their WT littermates. These results suggest a similar effect of ABHD15 on PDE3B expression in BAT. Hence, it could be possible that ABHD15-KO evocates insulin resistance in BAT as well as in WAT. However, further studies remain necessary in order to draw a complete picture of the role of Abhd15 in BAT and in whole-body energy metabolism.

Zusammenfassung

Übergewicht und Fettleibigkeit werden zu einem steigenden weltweiten Problem. Ein immer bequemerer Lebensstil in Kombination mit Überkonsum führt häufig zu Herz- und Kreislauferkrankungen. Dadurch steigerte sich das Interesse und intensivierte die Forschung über die Physiologie des Fettgewebes.

Fettgewebe kann in zwei verschiedene Arten mit unterschiedlicher Funktion unterteilt werden. Weißes Fettgewebe, welches vorrangig als Energiespeicher und -lieferant zur Verfügung steht und braunes Fettgewebe, das aus gespeichertem Fett Wärme erzeugt. Diese Arbeit beschäftigt sich mit dem α/ß hydrolase domain containing protein 15 (ABHD15) und dessen Rolle in braunen Fettzellen bzw. Fettgewebe. Bisher konzentrierten sich Forschungsarbeiten primär auf die Funktion von ABHD15 in weißen Fettzellen bzw. Fettgewebe. Die Zielstellungen dieses Projekts waren: 1) Die Auswirkung von systemischer Abhd15 Defizienz auf einzelne Gene und Prozesse im braunen Fettgewebe aufzuklären, 2) den Einfluss von Abhd15 auf immortalisierte braune Fettzellen in Bezug auf Zellproliferation und Zelldifferentiation zu untersuchen und 3) die Regulation von Abhd15 im braunen Fett von Mäusen aufgrund unterschiedlicher Ernährungszustände und in der Kälte zu analysieren.

Der erste Teil dieser Masterarbeit wurde mittels Microarray Experimenten und Genexpressionsanalysen realisiert. Auf diese Weise bekam ich interessante Ergebnisse bezüglich einer Fehlregulation von Genen und biologischen Prozessen im braunen Fettgewebe systemischer Abdh15 Knockout Mäuse. Die Ergebnisse weisen auf den Einfluss von Abhd15 auf biologische Prozesse hin, die den Energiehaushalt, Bildung reaktiver Sauerstoffspezies und den Hormonstoffwechsel regulieren. In einer immortalisierten braunen Adipozyten-Zelllinie, welche Abhd15 überexprimierte, untersuchte ich Zellproliferation und Zelldifferentiation. Leider konnte ich aufgrund eines Differenzierungsdefektes jedoch keine weiterführenden Analysen durchführen. Im dritten Teil fokussierte ich mich auf die Effekte von Abhd15 im braunem Fettgewebe von Mäusen mit unterschiedlichen Diäten, Ernährungszuständen und Umgebungstemperatur. Aktuelle Studien zeigten, dass ABHD15 stabilisierend auf die Phosphodiesterase 3B (PDE3B) wirkt und deren Expression im weißen Fettgewebe beeinflusst. Abhd15-defiziente Mäuse zeigten eine reduzierte PDE3B Expression. Dies führt zu einer ungehemmten Fettsäuremobilisierung und reduzierten Glukoseaufnahme, welche in einer Insulinresistenz endet. Meine Ergebnisse mit reduzierter PDE3B Expression im braunen Fettgewebe Abhd15-defizienter Mäuse deuten

darauf hin, dass ABHD15 im weißen und braunen Fettgewebe eine ähnliche Funktion ausüben könnte. Weiterführende und vertiefende Studien sind notwendig, um die Rolle von Abhd15 und deren Einflüsse im braunen Fettgewebe vollständig zu verstehen.

Acknowledgements

First, I would like to express my great appreciation to Assoc. Prof. Dr. Juliane Bogner-Strauss for giving me the opportunity to perform this master thesis in her laboratory and to be available for upcoming questions at any time. For me as a biomedical engineering student, this was a great chance to acquire practical as well as theoretical knowledge about lipid metabolism and laboratory skills.

Further I want to thank Xia Wenmin to introduce me into the lipid metabolism topic and to guide me through my first weeks in the lab, beside her own work.

Special thanks I want give to Melina Amor, who helped me out in times of need and supported me in many ways during my work on the thesis. She always took her time for me to answer my questions and helped me with the experimental setup, or the experiment itself, I needed to perform.

Next, I want to honor the help of Dina Hofer, Gabriel Zirkovits, Katharina Küntzel and Katharina Walter in terms of experimental advice or the answers of specific questions. Also, I want to thank all other members of this group who supported me with their expertise.

In addition, I want to acknowledge Thomas Schreiner and Wolfgang Krispel who made me familiar with many laboratory techniques and were ready to respond to any upcoming question.

Furthermore, I also want to acknowledge Dagmar Kratky, who supported me with her expertise and gave me very constructive inputs and comments for this master thesis.

Last but not least I want to thank my family and friends who supported me during my study and my master thesis.

Thank you!

Content

1 Introduction

1.1 Obesity, white and brown adipose tissue

In the last years, obesity turned out to be an ascending global problem, which has triplicated since the seventies. In 2016, approximately two billion adults aged 18 years and above were classified as overweight with more than a quarter being ranked as obese [1]. Obesity and overweight are defined by an excessive accumulation of fat that possibly compromises health. Both morbidities are commonly determined by the body mass index (BMI), which represents the weight of a person in kilograms in ratio to the height in square meters (kg/m^2). According to the World Health Organization (WHO), overweight is associated to BMI values > 25, while a BMI > 30 indicates obesity [1]. The general cause of obesity is an imbalance between calorie intake and energy expenditure. Worldwide, the rise of physical inactivity and excess of energy-dense nutrition have led to an increased morbidity of cardiovascular diseases, diabetes, musculoskeletal disorders, and even some cancers. Hence, an increased BMI is a primary risk factor of these non-communicable diseases [1].

Adipose tissue (AT) is the major biological energy reservoir playing a crucial role in the development and effects of obesity [2]–[4]. Alterations in the quantity and extent of fat mass can occur by hypertrophy or hyperplasia, respectively (Figure 1). Hypertrophy increases the adipocyte cell size and leads to dysfunctional adipocytes, often accompanied by increased insulin resistance, hypoxia and fibrosis, immune cell recruitment, and free fatty acid (FFA) release [2], [5]. Further, polarization of macrophages into classically activated pro-inflammatory M1 AT macrophages (ATM) might be involved in the increase of adiposity, leading to an imbalance among M1 and alternatively activated anti-inflammatory M2 ATMs. Whereas M1 macrophages promote AT insulin resistance and inflammation, M2 macrophages play a protective role by suppressing M1 function [5].

In contrast, hyperplasia is characterized by an increase in adipocyte number due to an increase of precursor cells differentiating into adipocytes. This maintains insulin sensitivity and counteracts FFA release, hypoxia and fibrosis, immune cell recruitment, and even adipocyte death [5].

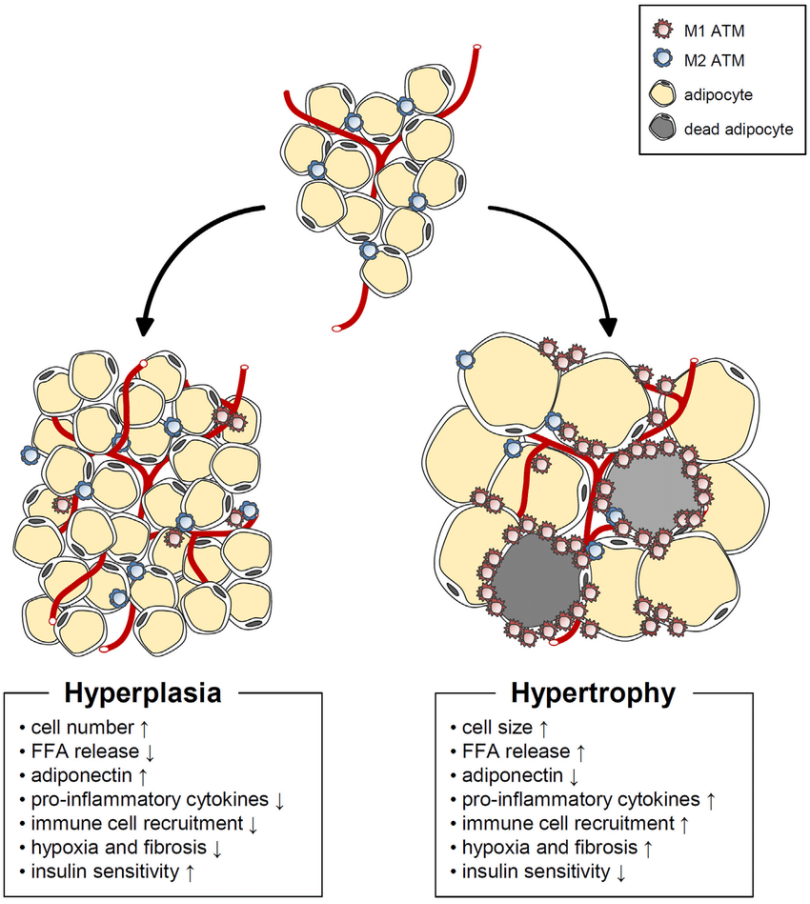

Figure 1: ***Two types of AT expansion:*** *Good natured hyperplasic adipose tissue expansion on the left-hand side and hypertrophic adipose tissue on the right-hand side* [5].

Mammals possess at least two types of AT which can be distinguished: white AT (WAT) and brown AT (BAT) [2]–[4]. During fasting or under calorie restriction, WAT serves as energy provider by releasing FFA. WAT has the potential to store vast amounts of energy in form of cytosolic lipid droplets (LD). In the case of white adipocytes, the energy is stored unilocular, meaning that one big LD is formed. However, WAT is far more than just a depot for energy storage. Over the last years, WAT became a widely recognized secretory organ that releases adipokines, which are able to control diverse physiological processes [3], [4], [6].

In contrast to WAT, BAT stores triglycerides in form of multilocular LDs, which enables faster availability for FA oxidation. Furthermore, brown adipocytes have a higher number of mitochondria than white adipocytes. The increased amount of mitochondria in BAT is responsible for its brown appearance. Exclusively BAT mitochondria express uncoupling protein 1 (UCP1) that characterize this tissue [7], [8].

In the inner membrane of mitochondria, UCP1 is capable to uncouple the mitochondrial respiratory chain from the adenosine triphosphate synthesis. As a result, BAT dissipates energy to generate heat in response to cold exposure. Therefore, the main function of BAT is

to sustain the body temperature by a process named nonshivering thermogenesis [9]. Another characteristic of BAT is the activation of its thermogenic function by the stimulation of β-adrenergic receptors by several agonists such as norepinephrine [10].

Lineage tracing studies revealed that white and brown adipocytes have a different origin. Brown adipocytes arise from myogenic factor 5 (MYF5) positive precursors, while white and beige adipocytes originate from the MYF5 positive and negative precursors (Figure 2) [7], [8], [10].

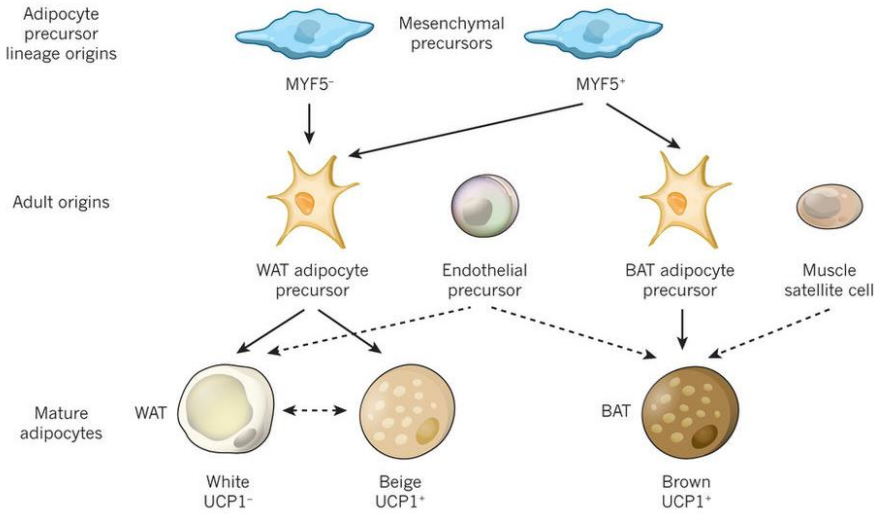

Figure 2: ***Overview of adipocytes origin.*** *Brown adipocytes arise from myogenic factor 5 (MYF5) positive precursors, while white and beige adipocytes originate from the MYF5 positive and negative precursors* [7].

The finding of a new type of adipocytes in fat depots led to the division of adipocytes into three classes: white, brown, and beige fat [3]. Under cold exposure or beta adrenergic stimulation, beige adipocytes are developed inside white fat depots, which is also referred as browning [10]. Beige adipocytes are also called brite (**br**own-in-wh**ite**) or inducible brown adipocytes [3], [10]. Brite adipocytes are distinct from the two other types of adipocytes. Nevertheless, they also share common characteristics like the same origin with the white adipocytes or their thermogenic function from brown adipocytes. This leads further to a typical higher UCP1 expression, which is also a hallmark of the browning process [3], [8], [10].

In addition to UCP1, PR domain containing 16 (PRDM16) is also considered as a BAT marker. PRDM16 regulates several genes contributing to thermogenesis in brown and beige adipocytes [5], [11]. Further, PRDM16 influences the activity of peroxisome proliferator-

activated receptor gamma coactivator 1- alpha (PGC-1α), which also likely plays a main role in thermogenesis [3].

Regarding the AT location in adult humans, WAT can be found in subcutaneous and visceral depots, especially enclosing intra-abdominal organs, while BAT is located around the shoulders and ribs [5]. The most common area where BAT could be detected is supraclavicular, whereas paravertebral and para-aortic appearances just occur occasionally (Figure 3) [12]. Compared to adults, the brown fat depots of infants are located interscapular and perirenal. Further distinguished differences in term of locations exist between humans and rodents, whereas WAT is also distributed in visceral and subcutaneous depots. Humans are missing the gonadal depots only existing in mice. BAT on the other hand is better developed and easier to observe in rodents with common locations in the neck and the interscapular area [2], [5], [12], [13].

Clinically, the determination of quantity and metabolic activity of BAT in humans is performed by positron emission tomography technique [14].

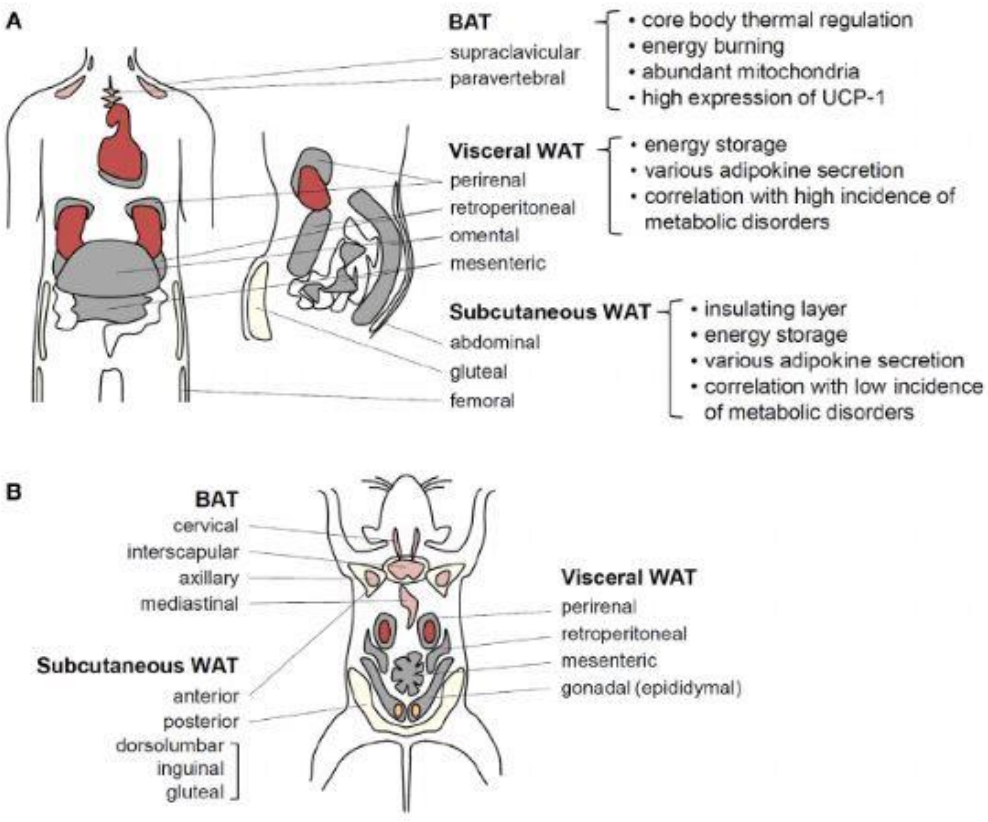

Figure 3: ***Distribution of WAT and BAT in humans and mice****. A) AT depots distribution in humans; B) AT depots distribution in mice* [5].

1.2 Differentiation of adipocytes, lipolysis, and lipogenesis

Mature adipocytes constitute approximately one third of the AT [6]. The other cell types that can also be found in this tissue are fibroblasts, preadipocytes, blood cells, endothelial cells, macrophages, and nerve tissue [6], [11]. Preadipocytes hold the ability to differentiate into mature adipocytes. During this process, preadipocytes, which have a fibroblast morphology, become spherical cells filled with LDs [6], [15].

Adipogenesis can roughly be divided in two phases. The first step is known as determination, where a stem cell commits to an adipocyte lineage, giving up the ability to differentiate into other cell types. Terminal differentiation is the second phase, when preadipocytes become mature fat cells [16], [17]. An extensive transcriptional cascade is set off for the molecular regulation of terminal differentiation. The transcriptions factors CCAAT/enhancer binding proteins (C/EBPs) and peroxisome proliferation-activated receptor γ (PPARγ) are key players associated with differentiation that directly affect adipocyte development [11], [17], [18]. Moreover, PPARγ and particularly the alpha isoform of the C/EBP family initiate the expression of genes which have important roles in adipocyte processes like lipogenesis, insulin sensitivity, and lipolysis. In addition, these genes encode specific proteins such as glucose transporter 4 (GLUT4), perilipin (PLIN1), fatty acid-binding protein 4 (FABP4), lipoprotein lipase (LPL), and the adipokines leptin and adiponectin [18].

Often referred as the “master regulator” of adipogenesis, PPARγ has two major isoforms: PPARγ1 and PPARγ2, the latter one differs from the first in an additional amino-terminal domain of 30 amino acids [11], [19]. Ren et al. showed that by endogenous PPARγ gene suppression in cells only ectopic PPARγ2 expression is able to save the adipogenic phenotype in the absence of PPARγ1, but not vice versa [19]. Further, PPARγ-deficient fibroblasts showed that C/EBPα alone cannot maintain differentiation; nevertheless, it still provides a significant assisting role. To date, no other candidate has been found to promote adipogenesis PPARγ-deficient conditions in fibroblasts [17].

In the center of the transcriptional cascade, which regulates adipocyte differentiation, PPARγ itself is the target of several pro- and anti-adipogenic factors, which directly or indirectly regulate its expression. Additionally, there are many supporting transcriptional factors, including PPARγ, which increase adipocyte development (Figure 4). Especially at the beginning of adipogenesis, C/EBPβ and C/EBPδ expression is quickly increased. Moreover, SREBP-1, a basic helix-loop-helix transcription factor, and the activator protein 1 (AP-1) are

pro-adipogenic. Members of the Kruppel-like family, for example, have both positive and negative influence on transcription (Figure 4) [11], [17].

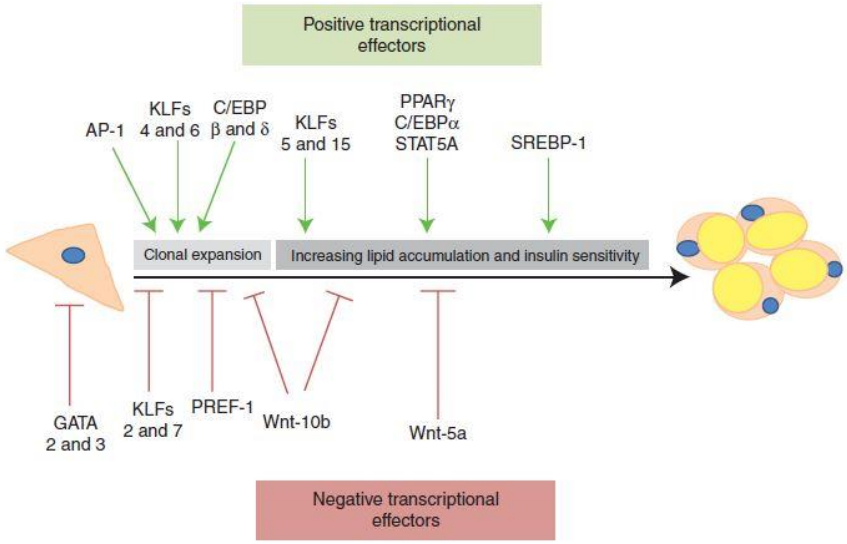

Figure 4: ***Transcription factors regulating adipocyte differentiation****. Transcription factors which have supportive (green) or inhibitory (red) influence on adipocyte differentiation [11].*

The essential mechanisms underlying adipocyte expansion and reduction are lipogenesis and lipolysis, respectively [2]. Lipogenesis refers to the process of energy storage as triglycerides (TGs) in LDs, while lipolysis comprises the energy mobilization by the hydrolysis of TGs [20]. Usually, energy is stored in the form of TGs, which consists of FAs esterified to a glycerol backbone (Figure 5) [2], [21].

Lipolysis can be stimulated by noradrenaline through ß-adrenergic receptors. This leads to an increase of cAMP levels, which further activates the cAMP-depending protein kinase A (PKA). Subsequently, the phosphorylation of the LD membrane protein PLIN1 is triggered [7]. PLIN1 has a key role in the regulation of TG hydrolysis. During lipolysis, PLIN1 is unbound to comparative gene identification-58 (CGI-58), which is a coactivator of adipose triglyceride lipase (ATGL) [2]. For lipolysis, the first FA from the TG is hydrolyzed by the ATGL enzyme. In a second step, the diacylglycerol is hydrolyzed by hormone sensitive lipase (HSL). Finally, monoglyceride lipase (MGL) hydrolyzes monoacylglycerol into a third FA and a glycerol molecule. Thus, three FAs are available for energy gaining through ß-oxidation (Figure 5) [2], [7], [20].

Lipolysis is suppressed during the postprandial period, when insulin is present in the circulation [2], [20]. Insulin thereby activates the translocation of the GLUT4 transporter to

the plasma membrane leading to higher glucose uptake [2]. In the cytosol, glucose is metabolized into pyruvate, which has two possible destinies. First, one part of pyruvate gets subsequently metabolized into lactate, which leaves the adipocyte and binds to a G protein-coupled receptor in the outer part of its membrane. This process leads to a decrease in cAMP levels and reduction of lipolysis [2]. Excess pyruvate also flows through the tricarboxylic acid (TCA) cycle, leading to an increased citrate production, which is diverted for FA synthesis [2] (Figure 5).

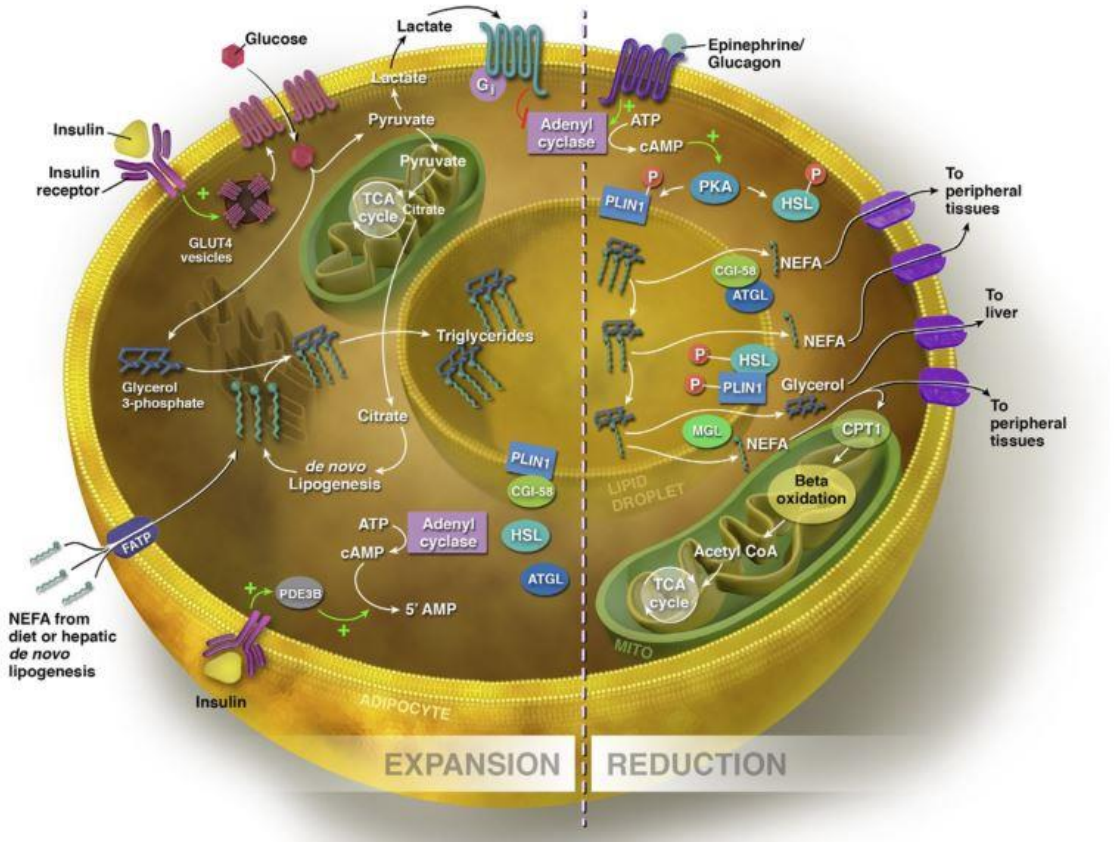

Figure 5: ***Adipocyte expansion and reduction****. An overview of processes and participants taking place in adipocyte enlargement and reduction* [2].

Further, insulin interacts through its receptor, followed by a signaling cascade, which raises the phosphorylation of phosphodiesterase 3B (PDE3B), thereby decreasing cAMP and hence PKA levels, which subsequently suppress lipolysis [2].

In WAT, an interaction between α/ß hydrolase domain containing protein 15 (ABHD15) and PDE3B could be detected, in which ABHD15 stabilizes PDE3B and influences its expression. AT-specific knockout mice with deletion of ABHD15 in WAT showed a reduced expression of PDE3B and induced an unrestrained FA mobilization, accompanied by a reduced glucose uptake which promotes insulin resistance [22].

These data strongly suggest ABHD15 as an interesting player in insulin signaling and resistance.

1.3 ABHD15

The mammalian α/ß hydrolase domain-containing protein (ABHD) superfamily consists of at least 19 proteins, including proteases, lipases, esterases, dehalogenases, peroxidases, and epoxide hydrolases [23]. Structurally, they share a characteristic fold composed of eight ß-strands, which are encircled by α-helices (Figure 6) [23].

ABHD proteins play a role in hydrolyzing molecules, which are participating in signal transduction and lipid metabolism. This hydrolase activity is achieved by a catalytic triad consisting of nucleophile-acid-histidine residues [23].

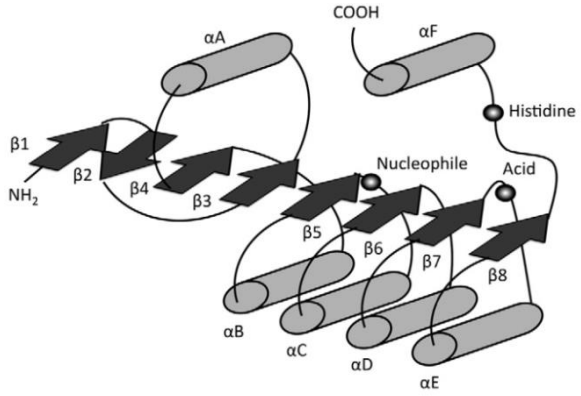

Figure 6: ***Structure of the α/ß hydrolase fold.*** *The eight mainly parallel ß-sheets are represented as arrows, whereas the α-helices are denoted as cylinders. Also included is the nucleophile-acid-histidine catalytic triad shown as spheres* [23].

ABHD15 belongs to the ABHD superfamily. In mice, it shows a vast expression in WAT and BAT as well as in skeletal muscle and liver [23]. The location of *Abhd15* in humans is on chromosome 17 (17q11.2). This gene encodes for a 468 amino acids protein with an expected molecular weight of ≈51 kDa [24], [25]. Obtaining a 90 % protein similarity (Protein BLAST outcome), the murine *Abhd15* is located on chromosome 11, which encodes a 459 amino acids protein having a size of ≈50 kDa [26], [27]. Since ABHD15 is missing the nucleophile residue, a hydrolytic function is unlikely and the prediction of its biochemical function is difficult [23].

Previous studies from our laboratory revealed that *Abhd15* is a target gene of Pparγ, which is highly upregulated during differentiation of 3T3-L1 cells and upon the Pparγ agonist rosiglitazone exposure [28]. Further, the absence of Abhd15 in those cells led to a

differentiation defect and compromised proliferation mechanistically by apoptosis. Additionally, an apoptosis-protecting role of ABHD15 has been suggested, since apoptosis induced with palmitic acid increased Abhd15 expression [28].

Studies so far focused mainly on Abhd15 in WAT or white adipocytes [22], [28]. Therefore, the main aims of this thesis were to:

- **Elucidate potential effects of constitutive Abhd15 knockout at the single gene and pathway levels in BAT;**
- **Investigate the role of Abhd15 in immortalized brown adipocytes during proliferation and differentiation;**
- **Analyze the regulation of Abhd15 in murine BAT upon different nutritional conditions or cold exposure.**

2 Materials

2.1 Cell culturing

Cell lines:

iBACs: SV40 T-large antigen immortalized brown adipose cell line

Phoenix: human embryonic kidney cell line, retroviral expression system

Reagents:

- Dimethylsulfoxide (DMSO); Sigma-Aldrich H. GmbH
- Dexamethasone (Dex); Sigma-Aldrich H. GmbH
- Foetal Bovine Serum (FBS); Lonza Inc.
- HEPES (4-(2-hydroxyethyl)-1-piperazineethanesulfonic acid); Life Technologies, Invitrogen corp.
- Hexadimethrine-bromide (Polybrene 8 mg/mL); Sigma-Aldrich H. GmbH.
- Indomethacin; Sigma-Aldrich H. GmbH
- Insulin (10mg/ml); Sigma-Aldrich H. GmbH
- 3-isobutyl-1-methylxanthine (IBMX, 1g); VWR International (Merck Chemicals)
- Isoproterenol; Sigma-Aldrich H. GmbH
- L-Glutamine (L-Glut) 200 mM; Life Technologies, Invitrogen corp.
- Metafectene; Biontex Laboratories GmbH.
- Penicillin/Streptomycin (P/S) Sol 10.000 U/ml per 10.000 µg/ml; Life Technologies, Invitrogen corp.
- Phosphate buffered saline (PBS, pH 7,4); Life Technologies, Invitrogen corp.
- Triiodothyronine (T3); Sigma-Aldrich H. GmbH
- 0,5 % Trypsin / EDTA (10x); Life Technologies, Invitrogen corp.

Culture media:

iBACs:

Growth Medium (GM)

Dulbeccos Modified Eagle Medium; Invitrogen corp.

DMEM + 4,5 g/l D-glucose, L-Glutamine + Pyruvate

+ 10 % FBS
+ 20 mM Hepes
+ 1 % P/S

Induction medium (IM)

GM

+ 20 nM Insulin (10 mg/ml stock)
+ 1 nM T3
+ 125 nM indomethacin
+ 500 nM Dexamethosone
+ 0,5 mM IBMX

Maintenance medium (MM)

GM

+ 20 nM Insulin
+ 1 nM T3

Freeze medium (FM)

9 % GM v/v

81 % FBS v/v

10 % DMSO v/v

Phoenix:

Standard Growth Medium (StdM)

Dulbeccos Modified Eagle Medium; Invitrogen corp.

DMEM + 4,5 g/l D-glucose, L-Glutamine + Pyruvate

+ FBS 10%
+ L-Glut 2 mM
+ P/S 100 U/ml / 100 µg/ml

Devices:

- BIO-RAD counting slides, dial chamber for cell counter
- BIO-RAD TC20 automated cell counter
- Microscope: Olympus CKX41
- Incubator: 37°C, CO_2 5%

2.2 Oil-Red-O staining

- "Ampura Spülllösung", Fresenius Kabi France
- 10 % formalin
- PBS
- Oil-Red-O Stock:

  0,25 g Oil-Red-O; ICN Bio

  50 ml Isopropanol

2.3 RNA isolation and quantification

Isolation:

"EXTRACTME® Total RNA kit"; BLIRT S.A. GDNANSK

- DEPC treated H_2O for molecular biology; Karl Roth GmbH + Co.KG
- Ethanol absolute; VWR

Quantification:

- DeNovix DS-11+ Spectrophotometer ("Nanodrop")

2.4 cDNA synthesis

High capacity cDNA Reverse Transcription kit; Thermo Scientific

Diethylpyrocarbonate (DEPC) added H_2O

Thermocycler peqSTAR; PeqLab

2.5 qPCR

Platinum® SYBR® Green; Invitrogen corp.

qPCR-primers:

	Forward	Reverse
mAbhd15	TATGAACGTGGGTTCTTGCT	TTGGTGTGACAGAACAGGGT
mCidea	TGACATTCATGGGATTGCAGAC	GGCCAGTTGTGATGACTAAGAC
mDio2	AACAGCTTCCTCCTAGATGCC	CATCAGCGGTCTTCTCCGAG
mUcp1	ACACCTGCCTCTCTCGGAAA	TAGGCTGCCCAATGAACACT
mPgc1α	TCTCTGGAACTGCAGGCCTAAC	TCAGCTTTGGCGAAGCCTT
mPparα	CCTGAACATCGAGTGTCGAATATG	GCGAATTGCATTGTGTGACATC
mPrdm16	TCCACAGCACGGTGAAGCCA	ATCTGCGTCCTGCAGTCGGC
mTf2β	TCAATAACTCGGTCCCCTACAA	GTCACATGTCCGAATCATCCA
mAtf3	CCCCGAGCGAAGACTGGAGCAAA	GGGACAATGGCGGTCGCACT
mAtf4	GTTGGTCAGTGCCTCAGACA	CATTCGAAACAGAGCATCG
mBip	CGGGCCGAGGAGGAGGACAA	ACACCGACGCAGGAATAGGTGGT
mChop10	GCAGCGACAGAGCCAGAATAAC	ACGTGGACCAGGTTCTGCTTTC
m36B4	TCCAGGCTTTGGGCATCA	CTTTATCAGCTGCACATCACTCAGA
mMss51	GAGACACTTCTGTGGGTGGG	GCCAGGCATCTGAAGATTTGC
mFlrt1	GACCGGGGACTCACATCCA	AGATTGATAGGGAACTCGTCCA
mRccd1	TGCCAGTGATGATATTTGCCAA	CCCCTGTAACGCAGAACCT
mLhfpl4	GCCTCGTCTTGGGCTGTATG	CCCACGAAATCTTTGTTCTCCTG
mStfa1	TCCTGTAGCCCAACTGTACCT	AGTGCCATCAGTTAGACCTGC
mMyl3	TGATGGCTGGTCAAGAGGAC	CTCCTCCCAAGAGCTTCACT

StepOne Software

StepOne Real Time PCR System

2.6 Protein isolation

Reagents:

- Protein inhibitor cocktail (PIC) tablets; Roche

Radio immunoprecipitation assay buffer (RIPA);

50 mM Tris-HCL (ph=7,5)

150 mM NaCl

1 % TritonX-100 v/v

0,5 % Na-deoxycholate v/v

0,1 % SDS v/v

dH_20

2.7 Protein quantification

- Pierce™ BCA protein assay kit; Thermo Scientific
- 0,9 % NaCl
- BIO RAD yMark, Microplate Spectrophotometer

2.8 Western blot

Primary antibodies: (Dilution)

anti-ABHD15; Proteintech (1:500)

anti-CC3; Cell Signaling (1:1000)

anti-GAPDH; Santa Cruz Biotechnology (1:1000)

anti-PDE3B; gift from Eva Degerman (1:500)

anti-PPARγ; Santa Cruz Biotechnology (1:500)

anti-TFIIb; Santa Cruz Biotechnology (1:1000)

anti-UCP1; Abcam (1:750)

anti-ß-ACTIN; (1:25000)

Secondary antibody: (Dilution)

anti-rabbit; Cell Signaling Technology (1:2000)

anti-mouse; GE healthcare UK Ltd. (1:2000)

Reagents:

- Bovine Serum Albumin (BSA); Roth GmbH + Co. KG
- Dithioerythritol (DTE); VWR International (Merck Chemicals)
- ECL prime; Amersham, GE Healthcare
- LDS sample buffer 4x; Life Technologies, Invitrogen corp.
- Light Ablot® PLUS; Euro Clone S.p.A
- Methanol Normapur for analysis; VWR International (Merck Chemicals)
- NuPAGE® Antioxidant; Life Technologies, Invitrogen corp.
- NuPAGE® MOPS SDS running buffer 20x; Life Technologies, Invitrogen corp.
- NuPAGE® 4-12 % Bis-Tris Gel 1,0 mm x 10 well; Life Technologies, Invitrogen corp.
- NuPAGE® 4-12 % Bis-Tris Gel 1,0 mm x 12 well; Life Technologies, Invitrogen corp.
- NuPAGE® 4-12 % Bis-Tris Gel 1,0 mm x 15 well; Life Technologies, Invitrogen corp.
- PBS, pH 7,4; Life Technologies, Invitrogen corp.
- Protease inhibitor cocktail tablets; Roche
- Powdered milk; Roth GmbH + Co. KG
- Restore Plus Western Blot Stripping Buffer, Thermo Scientific
- Sodium dodecyl sulfate (SDS); VWR International (Merck Chemicals)
- Seeblue® Plus2 Prestained Standard; Life Technologies, Invitrogen corp.
- Tris Glycine Buffer (TGS, 10x); Bio-Rad Laboratories GmbH
- Tween; VWR International (Merck Chemicals)

<u>20x MOPS running buffer:</u>

104,6 g MOPS

60,6 g Tris

10 g SDS

3 g EDTA

500 ml dH_20

pH should be 7,7

<u>Blocking solution:</u>

PBST or TBST

BSA 5 % or milk 5 %

10x PBS:

80 g NaCl (Sodium chloride)

2 g KCl (Potassium chloride)

11,5 g Na_2HPO_4 * $7H_20$ (Di-sodium phosphate heptahydrate)

2 g KH_2PO_4 (Potassium dihydrogen phosphate)

Fill up to 1000 ml with dH_20

Adjust pH value to 7,4

PBST:

10x PBS

0,05 % Tween 20

dH_20 1000 ml

10x TBS:

121,14 g Tris

87,66 g NaCl (Sodium chloride)

Fill up to 900 ml with dH_2O

Add 65 – 70 ml of 37 % HCL till pH value is 7,4

Fill up to 1000 ml with dH_2O

TBST:

10x TBS

0,05 % Tween 20

dH_20 1000 ml

TGS(10x):

30,29 g Tris

144,13 g Glycine

1 % SDS

Fill up to 1000 ml with dH_20

pH value 8,3

Transfer-buffer:

10 % TGS (10x)

20 % Methanol

dH_20 1000 ml

Syngene G: Box and Software

2.9 DNA isolation and quantification

Isolation:

Monarch™ PCR DNA Cleanup Kit, BioLabs® Inc.

- ddH_2O
- 70 % Ethanol

Quantification:

- DeNovix DS-11+ Spectrophotometer (“Nanodrop”)

2.10 Electroporation

Reagents:

- Electrolytic buffer (E2); Invitrogen corp.
- Resuspension buffer (T); Invitrogen corp.

Devices:

- Neon® transfection system; Invitrogen corp.
- Neon® pipette; Invitrogen corp.
- Neon® tips 100 µl; Invitrogen corp.

3 Methods

3.1 Analysis of BAT from Abhd15-KO and WT mice

3.1.1 Microarray analysis

For the hybridization, 200 ng of total RNA were hybridized on Mouse Gene 2.1 ST arrays (Affymetrix). Raw microarray data were analyzed by R package oligo, which is a preprocessing tool for oligonucleotide arrays. Normalization of the data was performed with robust multi-array average (RMA) method and log2-transformation. The probe sets were filtered for an inter-quartile range > 0,5 and the Refseq annotation filter as a reference for genome annotation. For the detection of differentially expressed genes (DEG), the R limma software package was utilized. Additionally, Benjamini-Hochberg method adjusted the p-values for multiple testing, considering if $p < 0,01$ and a false discovery rate (FDR) < 0,1. For the generation of the heatmaps, Genesis software (Sturn et al., 2002) was used.

3.1.2 Gene set enrichment analysis (GSEA):

Output primary raw data from the microarray experiment were uploaded to the gene set enrichment analysis (GSEA) software. The program was run with 1000 permutations and gene set as a permutation type, obtaining all dysregulated biological processes. All genes significantly contributing to the dysregulation of a pathway are called leading genes. Statistical significances were set at a nominal $p < 0,05$ and FDR $q < 25$ %. GSEA software was also used to perform selected leading genes heat maps, where higher expression values are represented with red and lower expression values with dark blue [29], [30].

3.2 Cell Culturing

3.2.1 Handling

For long time storage, cells were kept in cryovials with DMSO-containing freezing media and placed in liquid nitrogen tanks. To ensure a gentle freezing, the cells were stored in a freezing box containing isopropanol at -80 °C for about 24 hours before transferring them to the liquid nitrogen tanks. Thawing cells from the nitrogen tanks was executed by putting them immediately into the 37 °C water-bath, continuously shaking the cryovials for even distributed warming. When most of the content was liquid, cells were transferred into

already prepared flasks including pre-warmed growth medium (GM). The medium was changed within 24 hours to get rid of DMSO.

3.2.2 Cultivation

Proliferation of the cells was carried out in an incubator at 37 °C and 5 % CO_2. In order to ensure comparable growth, it was important that the cells were even distributed on the surface of the flask. This has been achieved by slewing the flasks in each direction during seeding. Proliferation was monitored under the microscope to avoid cells getting confluent, because this would interfere with their proliferation and differentiation potential.

3.2.3 Splitting

Cells were split at 60 - 80 % confluence. After removing the entire medium from the flask, cells were washed with PBS to guarantee that they were free from the GM. Subsequently, 1 ml trypsin solution was added to a 75 cm^2 flask to detach the cells from the flask surface. To reach an adequate effect of the trypsin, the culture vessel was put in the incubator or onto the heating plate (both at 37 °C) for 2 minutes. In order to inactivate trypsin, GM was added to the cells, because it contains FBS with protease inhibitors and stops trypsinization. Next, cells were distributed into new flasks. It was necessary to get rid of the trypsin, because in long term, trypsin is toxic for the cells. Thus, after inactivating trypsin, the suspension was transferred into 15 ml tubes and centrifuged for 5 minutes at 1200 rpm. The resulting pellet was resuspended in fresh medium for splitting.

3.2.4 Cell Passages

The cell passage number represents the number of how many times the cells were split or exposed to other stress situations like freezing and thawing, by increasing the passage number by one. Three samples, from the same cell line, with different cell passage numbers (for example p24, p25, p26) represent 3 biological replicates.

3.2.5 Differentiation procedure

Before cells reached 100 % confluence (between 90 - 100 %), adipogenesis was initiated by adding an induction medium for 48 hours. The whole differentiation process took 7 days. Differentiation medium was changed every 2 days. From day 5 on, the media was changed every day.

3.2.6 Cell proliferation assay

A number of 20.000 control and Abhd15 overexpressing (o/e) cells were seeded into a 6-well plate for comparison during proliferation. After 24, 48, 72 and 96 hours, cells were counted using a hemocytometer. A cell suspension of 10 µl was used to fill the counting chamber. Cells were counted under the microscope with 100X magnification.

3.3 Oil-Red-O staining

To explore the quantity of lipids and TGs in cells, I performed Oil-Red-O (ORO) staining. This method makes lipids and TGs visible as being colored in red. Control and Abhd15 o/e cells were cultured in 6-well plates and differentiation was induced. Cells were washed twice with PBS, fixed with 10 % formalin, and finally dried for 30 minutes. An ORO stock mixed with dH_20 in a 6:4 ratio was prepared and added to the cells. After 1 hour of incubation, stained lipids were visible in red under the microscope with 100X magnification.

3.4 RNA isolation from cells

Cells destined for RNA isolation were cultured in 12-well plates and harvested during different days of differentiation. For harvesting, cells were washed twice with PBS. Subsequently, 600 µl RNA lysis buffer was added on the cells. Shortly after, they were scratched off the plate and transferred into 1,5 ml Eppendorf tubes which were placed on ice. The RNA isolation procedure was performed according to the guidelines from the "EXTRACTME® Total RNA kit" datasheet. As an exception, the eluting step was done by adding 30 µl DEPC-H_2O to the RNA binding column, incubated at room temperature for 3 minutes, and centrifuged at 12.000 g for 2 minutes. This step was performed twice to increase the concentration of the eluate. RNA concentrations were measured with the "Nanodrop" device and samples were stored at -20 °C.

3.5 cDNA synthesis

The "high capacity cDNA reverse transcriptase kit" was used to reverse transcribe the isolated RNA into the copy DNA (cDNA) for further quantitative polymerase chain reaction (qPCR) analysis. The advantage of this process is that cDNA is double stranded and considerably more stable than RNA. Usually this serves as initial step in qPCR [31]. The mastermix contained 2 µl buffer, 2 µl random primers, 0,8 µl dNTP mix and 1 µl reverse transcriptase per sample. The mastermix was sniped and 5,8 µl where mixed with 1 µg of

RNA per reaction. Additionally, DEPC-H_2O was added to attain a final reaction volume of 20 µl per sample. Reverse transcription was performed as followed using a thermocycler device:

- 25 °C for 10 minutes
- 37 °C for 2 hours (optimal temperature for the reverse transcriptase)
- 85 °C for 5 minutes (enzyme deactivation)
- cDNA samples were diluted to a final concentration of 1 ng/µl with ddH_2O

3.6 qPCR

The qPCR is an advanced method for detection and quantification of nucleic acids. It is based on PCR, which is used for the amplification of DNA by three repeating steps (denaturation, annealing and elongation). Through fluorescent labeling it is possible to collect the data during the PCR [31].

The output of a qPCR is the number of cycles ("cycle threshold" CT value) reflecting a certain level of fluorescence, which is doubled in the exponential phase of the PCR after every cycle. After about 35 cycles, a plateau level is reached, meaning the intensity of the fluorescence is not further increasing. CT values are proportional to the initial cDNA amount of a sample. Thus, different CT values are representative for gene expression levels and can be compared by subtracting the CT value of a sample from the CT value of a reference sample. A delta CT value (ΔCT) of zero means that there is no difference in the gene expression of the target and the reference gene, yielding a ratio of one as seen in the following formula: [32]

$$2^{-(\Delta CT)} = 2^0 = 1$$

In this master thesis project, SYBR green was used as a fluorescent dye that unspecifically integrates into double stranded (ds)DNA. At 497 nm with the maximum excitation wavelength it absorbs blue light, while its fluorescence emission at 520 nm is green [33]. The template for the qPCR was generated with the StepOne software. Samples were prepared as followed: 4 µl cDNA, 4 µl of 800 nM primer mix (forward and reverse) and 8 µl SYBR green were pipetted together in 96-well plates.

Around 40 cycles of the following temperature profile were executed:

- 95°C for 10 min
- 95°C for 10s
- 60°C for 1 min

- 95°C 15s
- 60°C 1:30min
- 95°C for 15s

An evaluation of resulting CT values was done by using the double delta CT method, referenced to the housekeeping gene (here: TfIIb or m36B4).

3.7 Harvest and isolation from proteins

3.7.1 Harvest proteins from cells

To lyse the cells, 80 µl RIPA buffer including PIC per well were used. Immediately after adding the harvesting buffer, plates were incubated on a shaker in the 4 °C room for 30 minutes. As a next step, the cells were scratched off the plate and pipetted in an Eppendorf tube. During the harvesting process, the samples were kept on ice. Afterwards, the tubes were centrifuged for 30 minutes at 4 °C with 16.000 g. In that way, an upper fat layer and a lower layer containing cellular components were formed. To separate the protein from the before mentioned undesired layers, a hole was stung in the Eppendorf tube and the middle layer was transferred into a new tube. The isolated protein was stored on ice for further quantification analysis or put into the -20 °C freezer for future use.

3.7.2 Harvest proteins from tissue

Frozen murine tissue samples stored at -80 °C were transferred to dry ice and subsequently into 2 ml Eppendorf tubes, which contained approximately 100 µl (depending on the size of the tissue) of ice cold RIPA buffer including PIC. Afterwards, the specimens were kept on ice. The homogenization of the tissue was done with a hand blender. After every sample, the blender bar was first disinfected in 99 % ethanol and then washed in dH_2O to prevent contact between tissue and ethanol. Subsequently, the samples were put on ice for 20 minutes for cell lysis. The next step was the centrifugation of the sample at 4 °C for 10 minutes at 10.000 g. Further steps, such as the isolation of the protein, were already explained above.

3.8 Protein quantification

For the quantification of harvested protein fractions, a bicinchoninic acid (BCA) assay kit was utilized. This kit included two reagents A and B, bovine serum albumin (BSA) 2 mg/ml, which is a generally accepted protein reference for a total protein quantification, and 0,9 % NaCl.

Standard solutions of 20 µg, 15 µg, 10 µg, 5 µg, 2,5 µg and 0 µg (blank) BSA were prepared for the determination of protein concentrations. Both, the prepared standard row and the samples of which the protein amount had to be determined, were pipetted into a 96-well plate. A total volume of 212 µl per well was used containing in case of the standard row: 10 µl standard, 2 µl RIPA buffer (the reagent in which the sample was dissolved) and 200 µl of the working reagent composed of the reagents A and B from the kit in a proportion from 50:1. In case of the samples, 10 µl of 0,9 % NaCl, 2 µl sample and 200 µl working reagent were added. After incubation for 30 minutes at 37 °C, the absorbance at 562 nm was measured with a photospectrometer.

3.9 Western blot

After harvesting and isolation of the protein, the content was measured using the BCA kit as described above.

3.9.1 Gel electrophoresis

For the separation by size of the varying proteins in the samples, gel electrophoresis was done. According to the amount of protein obtained from the harvesting, 30-50 µg protein per sample, LDS and DTE were mixed together in an Eppendorf tube and filled up with dH_2O to the desired end volume. The quantity of LDS, DTE and dH_2O depended on the gel: for 10 well gels 30 µl and for 12 well gels, 20 µl per well were used. For denaturation of the proteins, the samples were heated at 70 °C for 10 minutes. Next, the specimens were short spun down in the centrifuge to recollect the vaporized fraction of the solution. The gels were prepared and placed into the western blot chamber and filled up with 600 ml running buffer. Different kind of gels and MOPS or MES running buffers were used (Figure 7). An antioxidant was added between the gels. Before loading the slots with the standard and the prepared samples, they were flushed by up- and down-pipetting. The gel then ran at 160-170 V for 60-70 minutes, depending on the kDa size of the desired protein.

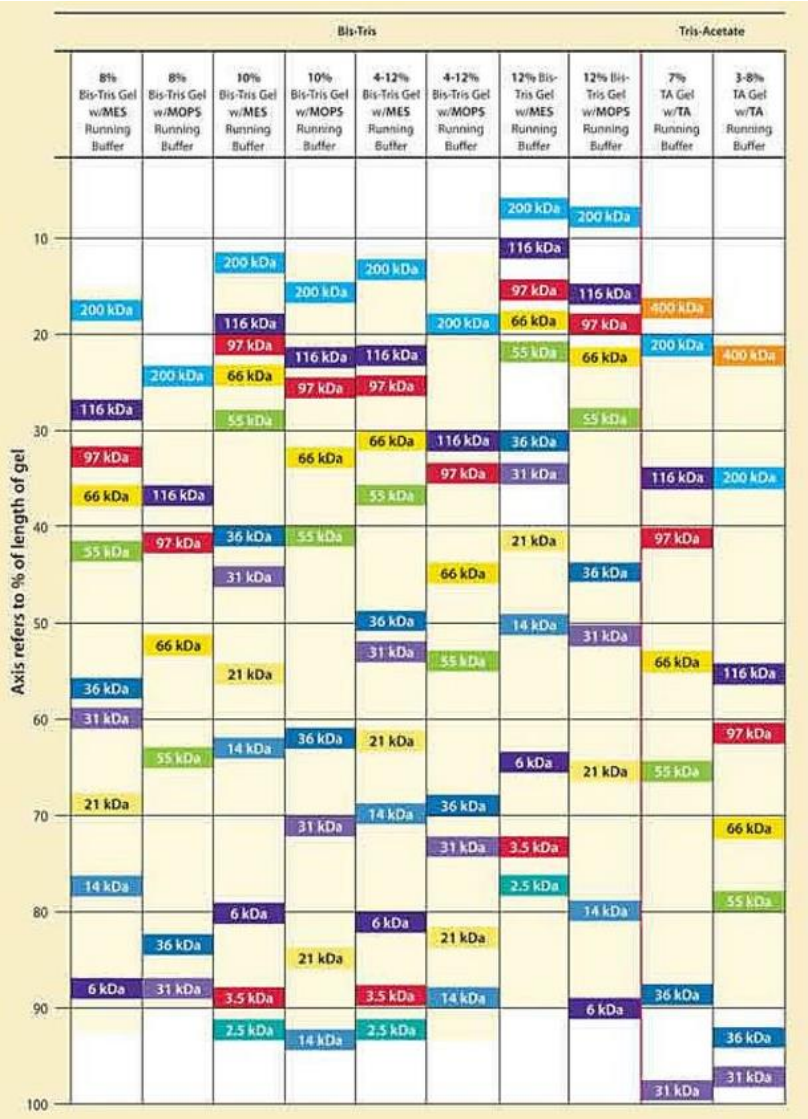

Figure 7: ***Migration patterns of protein standards****. Different separation patterns could be utilized depending on the gel and the running buffer* [34].

3.9.2 Transfer

Proteins were transferred from the gel onto a nitrocellulose membrane by their movement in an electrical field. The membrane was activated by placing it into a dish with dH_2O for a few minutes, meanwhile the transfer chamber was prepared. The gel and the membrane were placed in-between a transfer plate, using the following order: sponge, 2x filter papers, gel, membrane, 1x filter paper, sponge, executed in transfer buffer (Figure 8). Air-bubbles that would interfere with the transfer of the proteins were rolled out before closing the transfer plate. Afterwards, the transfer plate was placed in the chamber containing an ice block and a magnet stirrer. Subsequently, the transfer chamber was filled up with cold transfer buffer until the transfer plate was fully covered. The transfer was done at 500 mA

for 1,5 hours in the 4 °C room to ensure adequate cooling of the buffer. With the resulting blot, immune assays were performed.

Figure 8: ***Stack order for protein transfer****: Arrangement of the membrane and the gel in the transfer plate, ready for the transfer* [34].

3.9.3 PonceauS

PonceauS is a reversible staining that is used to visualize protein bands and allows to see if the proteins were successfully transferred from the gel to the membrane. The blot was incubated with PonceauS for 10 minutes and then washed with dH_2O five times to reduce the background signal and get rid of excess color. A picture of the blot was made with the imager.

3.9.4 Blocking

By blocking the membrane for 30 minutes up to 1 hour, unspecific antibody binding was prevented. The membrane was blocked in 5% BSA/milk dissolved in PBST/TBST solution.

3.9.5 Incubation with primary and secondary antibody

According to manufacturers' recommendations, the primary antibody was dissolved in the same blocking solution used for the blocking. Afterwards, the membrane was incubated with the primary antibody onto a rotor shaker at 4°C overnight. Incubation of the secondary antibody was carried out at room temperature for 2 hours. The secondary antibodies, either anti-rabbit or anti-mouse suitable to the primary antibodies, were dissolved 1:2000 in PBST or TBST. After every incubation, the membrane was washed 2 times for 10 minutes as well in PBST or TBST.

3.9.6 Detection

The detection of protein bands was performed by incubating the membrane between 3-5 minutes with chemiluminescent reagents in a 1:1 ratio. This has been done with GeneSys detection system and software. Blots could be incubated repeatedly with different primary antibodies by stripping them for 10-15 minutes, carefully washing the stripping buffer off and executing the points from blocking again.

3.9.7 Quantification

It was necessary to compare the determined protein levels to the so-called housekeeping protein. TFIIß, GAPDH or ß-ACTIN were used as housekeeping proteins for BAT. Western blot results were quantified by densitometry using ImageJ software and normalized to the housekeeping protein.

3.10 DNA isolation from Plasmid

DNA minipreps have been prepared in order to obtain plasmid DNA for the transfection and electroporation experiment. *E.coli*-glycerol stocks, either with the Murine Stem Cell Virus (pMSCV) vector containing the *Abhd15*-gene or the empty pMSCV-puromycin vector, were already available at our laboratory and stored at -80 °C. First, overnight cultures were prepared out of 10 µl glycerol-stocks in autoclaved Erlenmeyer flasks containing LB medium. Subsequently, ampicillin was added in a final concentration of 50 µg/ml. Cultures were grown on a shaker at 37 °C. On the next day, bacterial fractions were separated from the medium by centrifugation at 4500 g for 10 min. The resulting pellet was further treated with a miniprep kit for plasmid isolation, following the instructions as stated. Quantification of the purified isolated DNA was done with the Nanodrop device. Afterwards, the DNA was stored at -20 °C until usage.

3.11 Immortalized brown adipocytes

Abhd15 o/e and control cells were already available in the laboratory (generated by H. Pelzmann). These cells were generated as described below.

3.11.1 iBACs

Immortalization of cells is achieved by using the SV40 large T antigen on preadipocytes, separated out of the stromal vascular fraction of BAT from newborn mice [6], [17].

Simian virus 40 (SV40) is a protein possessing the large T antigen isoform, which compromises the cellular checkpoint mechanism of the host cell. This implies the deactivation of the cell division protecting system and therefore gaining “immortalization”, by enabling prolonged proliferation [35].

A retroviral plasmid vector including recombinant DNA (SV40 and puromycin resistance) was used to archive immortalization. Via transfection, the supernatant containing retrovirus particles were gained to infect isolated brown preadipocytes. Selection was performed using puromycin, consequently only cells with puromycin resistance, which have successfully integrated the recombinant DNA, survived. Thus, immortalized brown adipocytes were established.

3.11.2 iBACs Abhd15 o/e line cells already available in the lab

Abhd15 was cloned into a “plasmid Murine Stem Cell Virus” (pMSCV) vector. After transfecting Phoenix cells with that vector, viral particles were produced and further used to infect iBACs achieving a stable Abhd15 overexpression. Since during the immortalization steps the adipocytes already got puromycin resistance, a selection with puromycin was not possible. Hence, the cells had to be picked individually and tested for overexpression. The cells emerged out of manually selected cell 31 confirmed Abhd15 overexpression and will be further referred as iBACs Abhd15 o/e cells. For control cells, an empty vector with the antibiotic resistance gene was transfected.

3.12 Transfection

To transiently integrate foreign plasmid DNA into Phoenix cells, a transfection was performed using Metafectene. In order to promote an easy entry of the DNA into the cell, this transfection reagent modifies it to a compact structure and additionally destabilizes the lipid membrane coating the DNA/RNA.

For each well on a 6-well plate, a ratio of 2 µl Metafectene per 1 µg plasmid DNA was used. Consequential, one tube with the 1 µg of plasmid was filled up with 50 µl PBS and a second tube was prepared containing 2 µl Metafectene in 50 µl PBS. Afterwards, both were gently mixed together and incubated for 20 minutes at room temperature. After incubating, the

Metafectene-DNA complexes were pipetted dropwise onto the cells by holding the plate aslope and slewing it after every drop. The transfection was performed in the evening and on the next morning, the standard growth medium was changed to a fresh one. After 48 hours, the supernatant was collected and centrifuged to get rid of possibly unwanted cells. Transfection of Phoenix cells with pMSCV-Abhd15 or pMSCV-puro led to retroviral particles in the supernatant, which were further used for transduction.

3.13 Transduction

Transduction is a method to integrate foreign DNA into the genomic DNA of the desired cells using retroviral particles as carriers. To accomplish an Abhd15 o/e in iBACs, the cells were seeded into 6- and 12-well plates for analyses of protein and RNA expression, respectively. Transduction was started by adding 1 ml of the retroviral particles-enriched supernatant and polybrene at a final concentration of 6 µg/ml to the GM. Polybrene was used to increase the efficiency of the infection because it lowers repulsion forces amongst the virus and the cell, promoting the binding of retroviral particles to the cell surface [36]. For comparison, different situations were tested concerning the cell confluency and the number of infections (Table 1).

Table 1: Setting of the cell confluency and number of transduction

	Days of transduction			
Condition	1	2	3	4
Cell confluency	95 %	95 %	40 %	40 %
pMSCV Puro	d0	d0, d2	d0	d0, d2
pMSCV Abhd15	d0	d0, d2	d0	d0, d2

Differentiation was induced when cells reached 95 to 100 % confluency. Since polybrene can be toxic to the cells, additional wells were seeded with non-transduced cells to monitor the effect of this compound.

3.14 Electroporation

Another method for reaching an overexpression of Abhd15 in iBACs was the transfection of plasmid DNA into cells using electroporation. This method transiently increases the permeability of cell membranes. Due to a high electric field exposure, the membrane modifies its molecular structure and leads to the formation of pores, enabling molecules and ions to enter into the cell [37].

Cells were grown in 75 cm² flasks and harvested for counting. After centrifugation and removal of the supernatant, the pellet was resuspended with resuspension buffer. The wells were coated with gelatin solution and, after drying, filled up with 0,5 ml GM. For RNA evaluation, a 24-well plate was utilized. For harvesting protein, a 12-well plate with double amount of cells and DNA was used (Table 2).

Table 2: Settings for the electroporation experiment

Cell number per well/ RNA	150.000			
	Plasmid DNA concentration per well [µg]			
pMSCV Puro	0,5	0,5	0,25	0,25
pMSCV Abhd15	0,5	0,5	0,25	0,25
Cell number per well/ Protein	300.00			
	Plasmid DNA concentration per well [µg]			
pMSCV Puro	1	1	0,5	0,5
pMSCV Abhd15	1	1	0,5	0,5

As shown in Table 2, cells and plasmid DNA were pipetted together in tubes. Plasmid DNA and cells were mixed with the special Neon pipette and transferred to the electroporation camber from the Neon device. The chamber was filled with 3 ml of the electrolytic buffer. The settings on the Neon transfection system for the electroporation were adjusted to: 1400 V, 20 ms, 2 pulses. After the electrical field exposure, cells were pipetted in the already prepared plates and evenly distributed by shaking. Finally, the cells were incubated and induced at 95 – 100 % confluence.

3.15 Animal studies

All animal procedures followed the guidelines of the Austrian Federal Ministry of Science and Research and were approved by the institutional ethic committee. Mice tissues were already available in the laboratory and I used them for further analyses. Animals had *ad libitum* access to food (except during fasting) and water and were kept in a 14 hours light, 10 hours dark cycle. For overnight fasting, food was restricted in the dark cycle for around 12 hours. Mice were fed with chow diet (CD) (calories 11 kJ% from fat, 53 kJ% from carbohydrates and 36 kJ% from protein; #V1126, Ssniff Spezialdiäten, Germany) or specific diets were given to the mice at the age of 8 – 10 weeks:

- High glucose diet (HGD), calories 7 kJ% from fat, 72 kJ% from carbohydrates and 21 kJ% from protein (#E15629-34, Ssniff Spezialdiäten, Germany).
- High fat diet (HFD), 45 kJ% calories from fat, 35 kJ% from carbohydrates, and 20 kJ% from protein (#E15744-34 Ssniff Spezialdiäten, Germany).

3.15.1 BAT used for microarray experiment

BAT from 14 weeks old male mice fed with CD was harvested after overnight fasting and 1 hour of refeeding. This experiment included 5 whole-body Abhd15- knockout (KO) and 3 wild type (WT) mice.

3.15.2 Validation of microarray analysis

I validated the microarray data by qPCR with the same samples included in the microarray experiment. Additionally, I used samples from an independent mouse experiment which included BAT from 30 weeks old male mice fed with HFD and harvested after overnight fasting and refeeding. This experiment comprised 5 Abhd15-KO and 3 WT mice.

3.15.3 Fasting and cold exposure of Abhd15-KO and WT mice

Mice at the age of 27 weeks were first fasted and kept at 4°C for 90 minutes and subsequently sacrificed. BAT was harvested and snap frozen in liquid nitrogen. This experiment included 4 Abhd15-KO and 4 WT mice.

3.15.4 Cold exposure of mice

BAT was harvested from WT mice kept for 24 hours (n = 3) or 3 weeks (n = 4) at 4°C. Their respective controls were kept at room temperature (RT) (n = 3).

3.15.5 Dietary experiments

BAT from 20 weeks old WT mice (n=2) on CD was harvested after overnight fasting and 1 or 2 hours of refeeding. BAT was also harvested from mice fed with CD (n = 2), HGD (n = 3) or HFD (n = 3) in the fed state.

3.16 Statistical analysis

The two-tailed Student's-t-test was applied for investigation of statistical significance with probability values given as followed: * $p \leq 0,05$; ** $p \leq 0,01$; *** $p \leq 0,005$; **** $p \leq 0,001$. All results show the mean value and the standard deviation.

4 Results

4.1 Microarray experiment

In order to elucidate potential dysregulated genes and pathways in response to Abhd15 deficiency, I performed a microarray experiment with BAT from WT or whole-body Abhd15-KO mice fed with CD.

4.1.1 Microarray analysis BAT Abhd15-KO vs WT mice

Data were analyzed as described in the methods section. Overall, 41.345 probes were analyzed and 60 differentially expressed genes (DEG) were significantly deregulated with a p value ≤ 0.05. Out of them, 28 genes were upregulated (fold change > 1,2) (Table 3) and 32 genes were downregulated (fold change < -1,2) (Table 4).

Table 3: List of significantly upregulated genes from the microarray analysis ordered by descending fold change values.

Gene symbol	Gene name	Fold change	p value
Mss51	*MSS51 mitochondrial translational activator*	1,93	0,0007
Krtap5-1	*Keratin associated protein 5-1*	1,76	0,0046
Flrt1	*Fibronectin leucine rich transmembrane protein 1*	1,70	0,0058
Rccd1	*RCC1 domain containing 1*	1,67	0,0067
Olfr1049	*Olfactory receptor 1049*	1,65	0,0052
Ccdc28b	*Coiled coil domain containing 28B*	1,63	0,0014
Uhrf1	*Ubiquitin-like, containing PHD and RING finger domains, 1*	1,61	0,0069
Myo1e	*Myosin IE*	1,60	0,0091
Trib2	*Tribbles homolog 2 (Drosophila)*	1,55	0,0022
Slc43a2	*Solute carrier family 43, member 2*	1,55	0,0032
Pla2g4b	*Hospholipase A2, group IVB (cytosolic)*	1,54	0,0007
Tmem79	*Transmembrane protein 79*	1,53	0,0061
Vwa5b2	*Von Willebrand factor A domain containing 5B2*	1,52	0,0012
Lpo	*Lactoperoxidase*	1,52	0,0047
Fgf18	*Fibroblast growth factor 18*	1,51	0,0067
Zfp182	*Zinc finger protein 182*	1,51	0,0082
Slc2a1	*Solute carrier family2 (facilitated glucose transporter), member1*	1,50	0,0014
Apoh	*Apolipoprotein H*	1,44	0,0060
F5	*Coagulation factor V*	1,44	0,0074
Tram2	*Translocating chain-associating membrane protein 2*	1,43	0,0070
Stbd1	*Starch binding domain 1*	1,43	0,0064
Scrn1	*Secernin 1*	1,41	0,0091
Prcp	*Prolylcarboxypeptidase (angiotensinase C)*	1,39	0,0058
Mat2a	*Methionine adenosyltransferase II, alpha*	1,36	0,0019
Traf1	*TNF receptor-associated factor 1*	1,36	0,0019
Mob3b	*MOB kinase activator 3B*	1,32	0,0042
Timp3	*Tissue inhibitor of metalloproteinase 3*	1,30	0,0062
Rai14	*Retinoic acid induced 14*	1,26	0,0099

Table 4: List of significantly downregulated genes from the microarray analysis ordered by ascending fold change values.

Gene symbol	Gene name	Fold change	p value
Lhfpl4	*Lipoma HMGIC fusion partner-like protein 4*	-2,15	0,0004
Stfa1	*Stefin A1*	-2,04	0,0002
Myl3	*Myosin light chain 3*	-1,97	0,0026
Hspb2	*Heat shock protein 2*	-1,92	0,0004
Ptgfrn	*Prostaglandin F2 receptor negative regulator*	-1,69	0,0086
Olfml1	*Olfactomedin-like 1*	-1,63	0,0053
Sprr1b	*Small proline-rich protein 1B*	-1,63	0,0018
Cand2	*Cullin-associated and neddylation-dissociated 2 (putative)*	-1,62	0,0026
Irc1	*Killer cell lectin-like receptor subfamily C, member 1*	-1,61	0,0061
Sema3c	*Semaphorin 3C*	-1,61	0,0065
Ar	*Androgen receptor*	-1,61	0,0066
Defa-rs12	*Defensin, alpha, related sequence 12*	-1,60	0,0054
Mvd	*Mevalonate (diphospho) decarboxylase*	-1,60	0,0045
Asgr1	*Asialoglycoprotein receptor 1*	-1,55	0,0001
Tradd	*TNFRSF1A-associated via death domain*	-1,53	0,0035
Ppcs	*Phosphopantothenoylcysteine synthetase*	-1,53	0,0038
Clec3b	*C-type lectin domain family 3, member b*	-1,52	0,0030
Cyp8b1	*Cytochrome P450, family 8, subfamily b, polypeptide 1*	-1,51	0,0056
Casp12	*Caspase 12*	-1,49	0,0028
Olfr1302	*Olfactory receptor 1302*	-1,49	0,0097
Epc1	*Enhancer of polycomb homolog 1 (Drosophila)*	-1,48	0,0033
Spon1	*Spondin 1, (f-spondin) extracellular matrix protein*	-1,47	0,0017
Igf1	*Insulin-like growth factor 1*	-1,43	0,0098
Harbi1	*Harbinger transposase derived 1*	-1,43	0,0051
Gatsl2	*GATS protein-like 2*	-1,43	0,0093
Cyp2c37	*Cytochrome P450, family 2. subfamily c, polypeptide 37*	-1,42	0,0065
Ift122	*Intraflagellar transport 122*	-1,42	0,0073
Znf512b	*Zinc finger protein 512B*	-1,35	0,0020
Nckipsd	*NCK interacting protein with SH3 domain*	-1,35	0,0074
Irf2	*Interferon regulatory factor 2*	-1,32	0,0099
Trf	*Transferrin|signal recognition particle receptor, B subunit*	-1,28	0,0045
Cyp2e1	*Cytochrome P450, family 2, subfamily e, polypeptide 1*	-1,24	0,0045

A graphical representation of the dysregulated genes in BAT from Abhd15-KO in comparison to their WT controls can be seen in the heatmaps (Figure 9). The upregulated genes are depicted in red and the downregulated ones in blue. The top three upregulated genes were *mitochondrial translational activator* (*MSS51*), *keratin associated protein 5-1* (*KRTAP5-1*) and *fibronectin leucine rich transmembrane protein 1* (*FLRT1*), with fold changes of 1,93, 1,76 and 1,70, respectively. On the other hand, the top three downregulated genes were *lipoma HMGIC fusion partner-like protein 4* (*LHFPL4*), *stefin A1* (*STFA1*) and *myosin light polypeptide 3* (*MYL3*) whith fold changes of -2,15, -2,04 and -1,97, respectively.

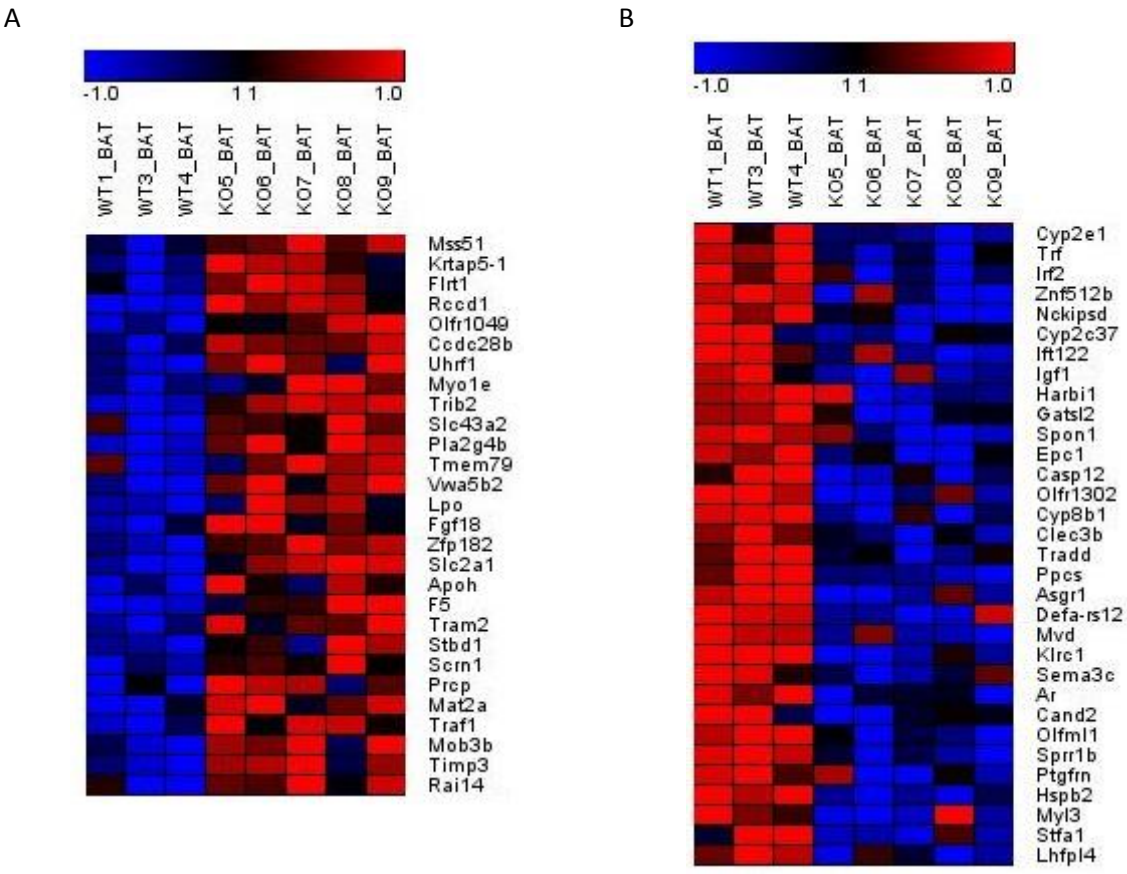

Figure 9: ***Heatmaps showing differentially expressed genes from the microarray analysis.*** *A) Significant upregulated genes in BAT from 3 WT and 5 Abhd15-KO mice; B) Significant downregulated genes in BAT from 3 WT and 5 Abhd15-KO mice. Upregulated genes are represented in red, downregulated genes in blue.*

Mss51 is a recently discovered gene mainly expressed in skeletal muscle. Genetic modification of the gene leads to raised glycolysis and FA oxidation on a cellular level. Human muscle MSS51 is located to the mitochondria [38]. Nothing has been reported so far regarding its role in BAT.

KRTAP5-1 belongs to the keratin-associated protein gene family, which is best known for the formation of a stiff and robust hair shaft. Therefore, the protein is found in the hair cortex, more specifically, hair keratin intermediate filaments consist of KRTAP [39]. So far, a function of KRTAP5-1 in BAT has not been described.

FLRT1 and generally the fibronectin leucine rich transmembrane protein family members participate in cell adhesion and receptor signaling [40]. The pathogenesis of autosomal recessive spastic paraplegia type 68 has been related to FLRT1, which is mainly expressed in brain and kidney [40]. No further connection of FLRT1 and its possible influence in BAT has been found so far.

LHFPL4 is part of the tetraspan transmembrane protein encoding genes with highest RNA expression in the brain. Mutations in one LHFP- like gene have been linked to a high mobility group gene, which is associated with a translocation causing benign adipocyte tumor, called lipoma [41].

Stefin A (STFA1), also named cystatin A, is a member of the cystatin superfamily and belongs to the cysteine protease inhibitors. STFA1 is mainly expressed in lymphoid and epithelial tissue [42]. A suggested function of STFA1 is protection of cysteine proteases and it may also have a possible role in apoptosis. Cysteine proteases can be released under certain conditions from lysosomes and degrade cytosolic and cytoskeleton proteins. Further, STFA1 may protect epithelial and lymphoid tissues, from raised cysteine proteases level caused through pathogens [42]. No connection between BAT and the function of STFA1 was found in the literature.

Especially expressed in muscle tissue, *Myl3* is associated with cardiomyopathy [43]. Recent studies showed that cardiovascular risk factors were modulated by functional BAT. It has been reported that the transplantation of WT BAT into UCP1-KO mice seemed to have a cardioprotective benefit [44].

4.1.2 Validation of the microarray data

Further, I proceeded to validate the data from the microarray experiment by qPCR. In order to do this, I included the same samples used for the microarray experiment and an additional set of samples from an independent mouse experiment. Since it was not possible to design a qPCR primer for *Krtap5-1*, *RCC1 domain containing 1* (*RCCD1*) gene, with a fold change of 1,67, was evaluated. In contrast to the microarray data, none of the genes were significantly dysregulated after qPCR analysis (Figure 10).

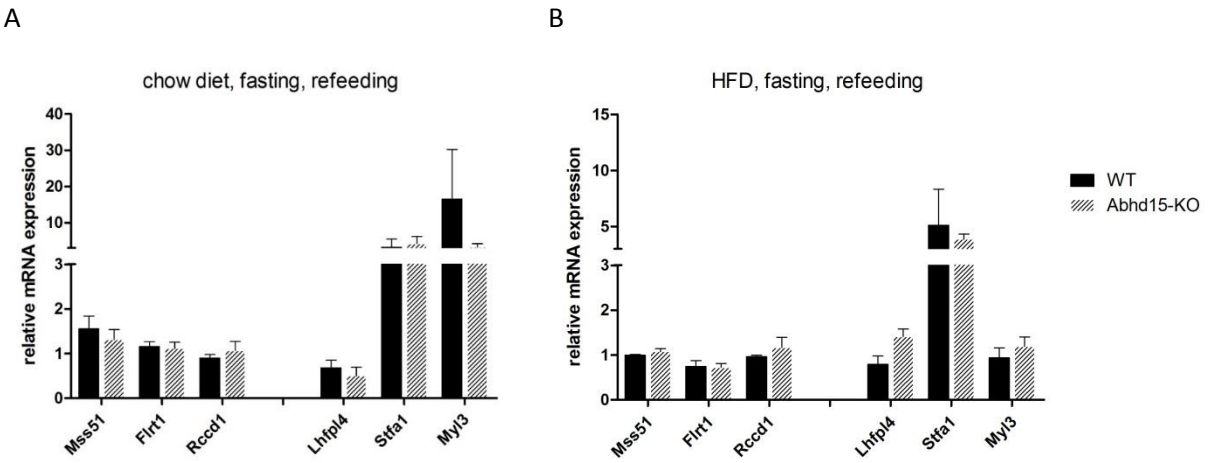

Figure 10: ***Microarray results validation by qPCR.*** *A) Samples from the microarray experiment; B) Samples from an independent animal experiment. Results include 3 wild type (WT) and 5 knockout (KO) mice and show the mean value ± standard deviation (sd).*

4.2 Gene set enrichment analysis

With the aim to elucidate dysregulated pathways in BAT of Abhd15-KO mice in comparison to WT mice, I performed GSEA. For this, I used the raw data from the microarray experiment as specified in the methods. In total, I found 31 upregulated and 48 downregulated biological processes. However, since this study was focused on BAT, I preselected all those dysregulated biological processes potentially associated to BAT metabolism and homeostasis for further analysis (Table 5).

Table 5: Dysregulated biological processes in Abhd15-KO. Highlighted in bold are the biological processes related to metabolism in BAT.

Upregulated	Downregulated
DNA methylation involved in gamete generation	Actin myosin filament sliding
Protein autoubiquitination	DNA catabolic process endonucleolytic DNA
Calcium dependent cell adhesion via plasma membrane cell adhesion molecules	Actin mediated cell contraction
CGMP biosynthetic process	Muscle contraction
Hydrogen peroxide metabolic process	Striated muscle contraction
Peripheral nervous system axon ensheathment	Muscle system process
Regulation of energy homeostasis	Muscle structure development
Negative regulation of cartilage development	Actin filament based movement
Camera type eye photoreceptor cell differentiation	Muscle organ development
Negative regulation of chondrocyte differentiation	Muscle cell development
Thyroid hormone metabolic process	Ovulation cycle process
Mitochondrial ATP synthesis coupled proton transport	**Regulation of superoxide metabolic process**
Negative regulation of cation channel activity	Cardiac muscle tissue morphogene
Phenol containing compound metabolic process	Dendritic cell migration
Amelogenesis	DNA catabolic process
Osteoblast development	Regulation of muscle adaption
Response to copper ion	Striated muscle cell differentiation
Neutral tube patterning	Heart process
Visual behavior	Muscle cell differentiation
Regulation of water loss via skin	Skeletal muscle organ development
Pigment granule organization	Myofibril assembly
Schwann cell development	Actin filament based process
Alcohol catabolic process	Myoblast differentiation
Energy coupled proton transport down electrochemical gradient	Regulation of calcium mediated signalling
Cerebral cortex cell migration	Cell aggregation
Organic hydroxy compound catabolic process	Response to dexamethasone
Retina homeostasis	Positive regulation of heart rate
Phospholipase C activating G protein coupled receptor signalling pathway	Positive regulation of endothelial cell migration

Continuing Table 5: Dysregulated biological processes in Abhd15-KO. Highlighted in bold are the biological processes related to metabolism in BAT.

Upregulated	Downregulated
Sensory perception of pain	Skeletal muscle contraction
Response to arsenic containing substance	**Negative regulation of steroid metabolic process**
Regulation of chondrocyte differentiation	Positive regulation of leukocyte chemotaxis
	Chemokine mediated signalling pathway
	Multicellular organismal movement
	Muscle tissue development
	Regulation of lymphocyte chemotaxis
	Positive regulation of steroid metabolic process
	Cellular component disassembly involved in execution phase of apoptosis
	Female sex differentiation
	Cardiac ventricle development
	Apoptotic nuclear changes
	Inflammatory response to antigenic stimulus
	Ovulation cycle
	Dendritic spine development
	Positive regulation of phosphatidylinositol 3 kinase signalling
	Cardiac muscle tissue development
	Ventricular cardiac muscle cell differentiation
	Ventricle morphogenesis
	Ventricular cardiac muscle tissue development

4.2.1 Hydrogen peroxide metabolic process

The hydrogen peroxide metabolic process comprises 30 genes [45]. *Cytochrome P450 family 1 subfamily A member 1* (*CYP1A1*), *lactoperoxidase* (*LPO*), *dual oxidase maturation factor 1* (*DUOXA1*), and *thyroid peroxidase* (*TPO*) were the leading genes in Abhd15-KO mice (Figure 11).

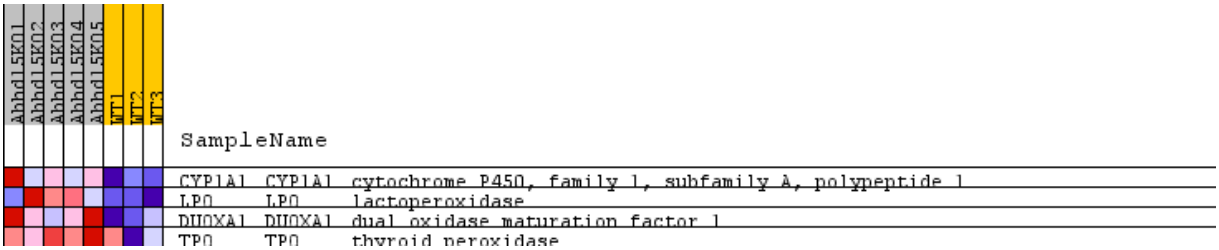

Figure 11: ***Leading genes heatmap for the H_2O_2 metabolic process.*** *Results include data from 5 Abhd15-KO and 3 WT mice. Higher expression values are represented in red and lower expression values in blue.*

4.2.2 Regulation of energy homeostasis

The regulation of energy homeostasis biological process involves 17 genes in total [47]. Out of them, 11 genes showed to lead to the dysregulation of this biological processes in BAT of Abhd15-KO mice (Figure 12). *Abhd15* deficiency dysregulates two-thirds of these genes, indicating that ABHD15 plays a role in the regulation of energy homeostasis of BAT.

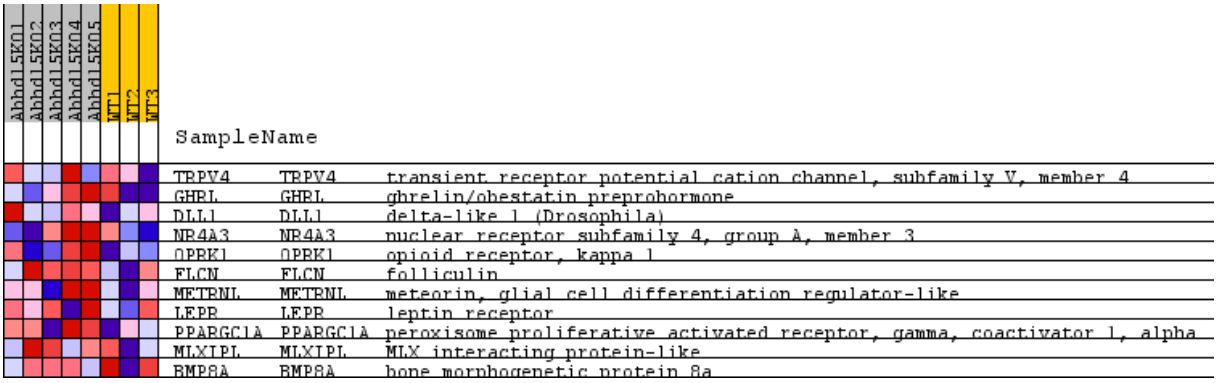

Figure 12: ***Leading genes heatmap for the energy homeostasis biological process.*** *Results include data from 5 Abhd15-KO and 3 WT mice. Higher expression values are represented in red and lower expression values in blue.*

4.2.3 Thyroid hormone metabolic process

The thyroid hormone metabolic process consists of 22 genes [50], whereas 7 of them significantly affected the whole pathway dysregulation in Abhd15-KO mice (Figure 13).

Thyroid hormones have a major role in the regulation of energy homeostasis. Prohormone thyroxine (T4) and its active form triiodothyronine (T3) play a central role in this biological process. A crucial enzyme included in the activation of this hormone is type 2 deiodinase (DIO2), which is mainly expressed in regions of the brain, BAT, and WAT [51], [52].

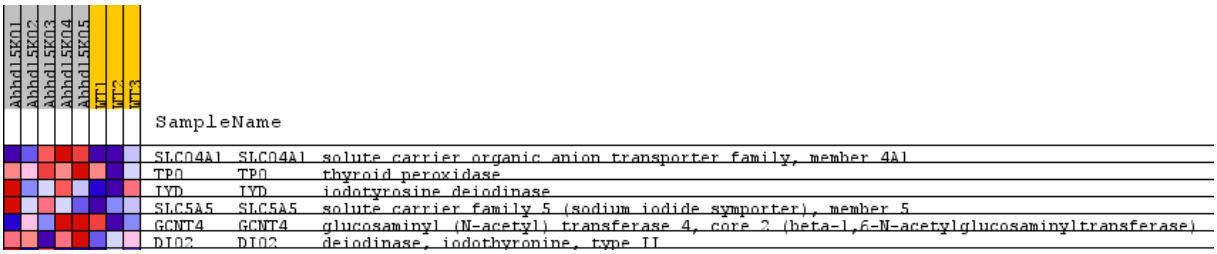

Figure 13: ***Leading genes heatmap for the thyroid hormone biological process.*** *Results include data from 5 Abhd15-KO and 3 WT mice. Higher expression values are represented in red and lower expression values in blue.*

4.2.4 Regulation of superoxide metabolic pathway

Regulation of superoxide metabolic pathway is defined by 23 genes. This biological processes refers to any pathway where superoxide (O_2^-) takes part, either as reagent or as product [55]. Six of these genes significantly affect the dysregulation of this pathway in the BAT of our mouse model (Figure 14).

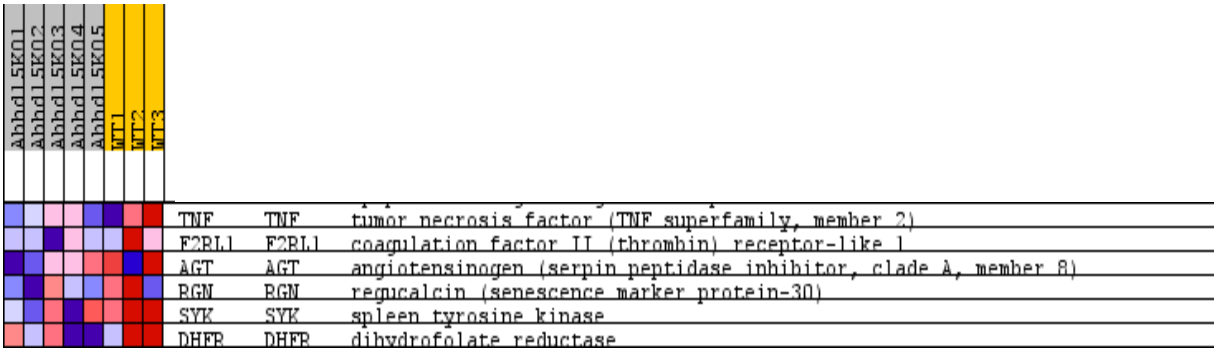

Figure 14: ***Leading genes heatmap for the superoxide metabolic pathway.*** *Results include data from 5 Abhd15-KO and 3 WT mice. Higher expression values are represented in red and lower expression values in blue.*

4.2.5 Negative and positive regulation of steroid metabolic process

The negative steroid metabolic process is regulated by 24 genes. This pathway involves genes that deactivate other pathways where steroids play a role [57]. Out of the 23 genes involved in this pathway, I found 10 being responsible for the dysregulation of the whole pathway when comparing Abhd15-KO to WT mice (Figure 15).

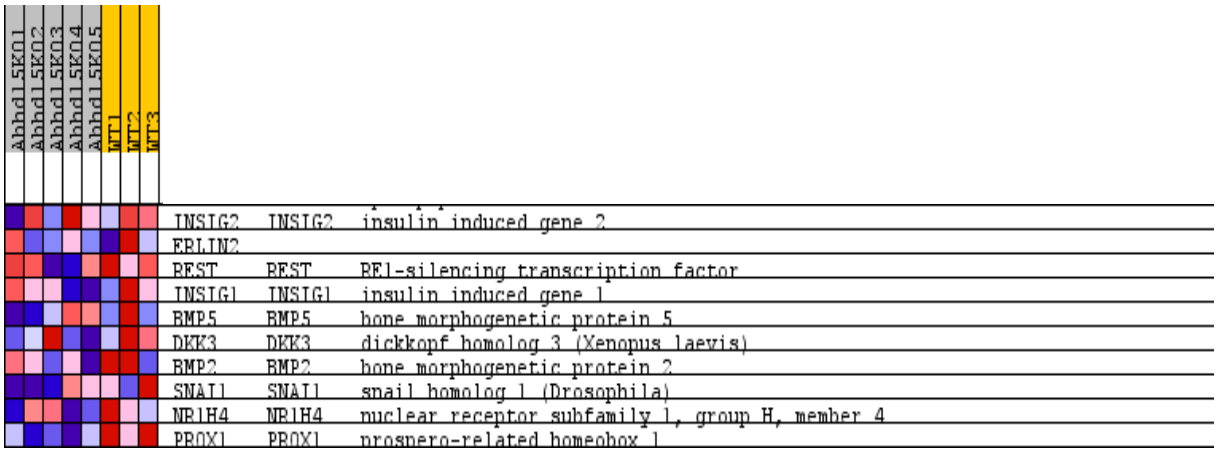

Figure 15: ***Leading genes heatmap for the negative steroid metabolic process.*** *Results include data from 5 Abhd15-KO and 3 WT mice. Higher expression values are represented in red and lower expression values in blue.*

The positive steroid metabolic process is regulated by 23 genes. This pathway involves genes that activate other pathways where steroids play a role [58]. Out of the 23 genes involved in this pathway, I found 11 being responsible for the dysregulation of the whole pathway when comparing Abhd15-KO to WT mice (Figure 16).

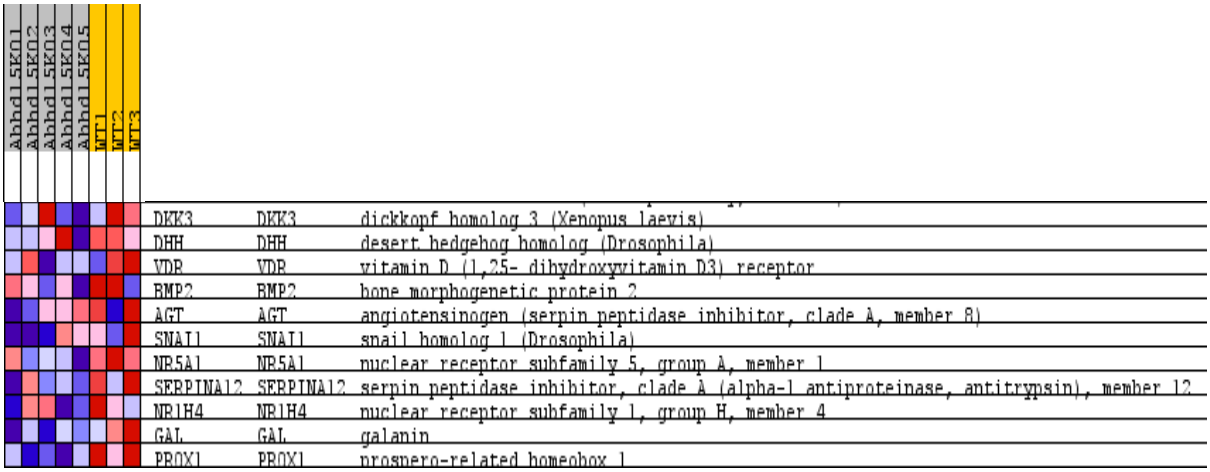

Figure 16: ***Leading genes heatmap for the positive steroid metabolic process.*** *Results include data from 5 Abhd15-KO and 3 WT mice. Higher expression values are represented in red and lower expression values in blue.*

4.3 Role of Abhd15 in immortalized brown adipocytes (iBACs) during proliferation and differentiation

4.3.1 Differentiation and ORO staining of Abhd15 o/e iBACs

To find out more about the role of ABHD15 in BAT, I performed experiments with iBACs overexpressing *Abhd15*. I studied these cells deeply during its whole differentiation process by utilizing different cellular and biochemical analysis.

First, I differentiated three biological replicates (p24, p25 and p26) of control and Abhd15 o/e iBACs from day 0 to day 6. During differentiation, I took pictures under the light microscope (Figure 17). Importantly, I detected a differentiation defect in Abhd15 o/e iBACs during change of the differentiation media after 48 hours of induction. This defect was evidenced by the detachment and/or death of the cells (Figure 17).

In contrast, control cells fully differentiated into mature adipocytes, which has been denoted by the deposition of LDs evidenced by the red color as a product of the ORO staining (Figure 18). Abhd15 o/e cells appeared to keep on proliferating, which was indicated by a fully covered surface of the well with cells at day 6, without the differentiation capacity (Figures 17, 18).

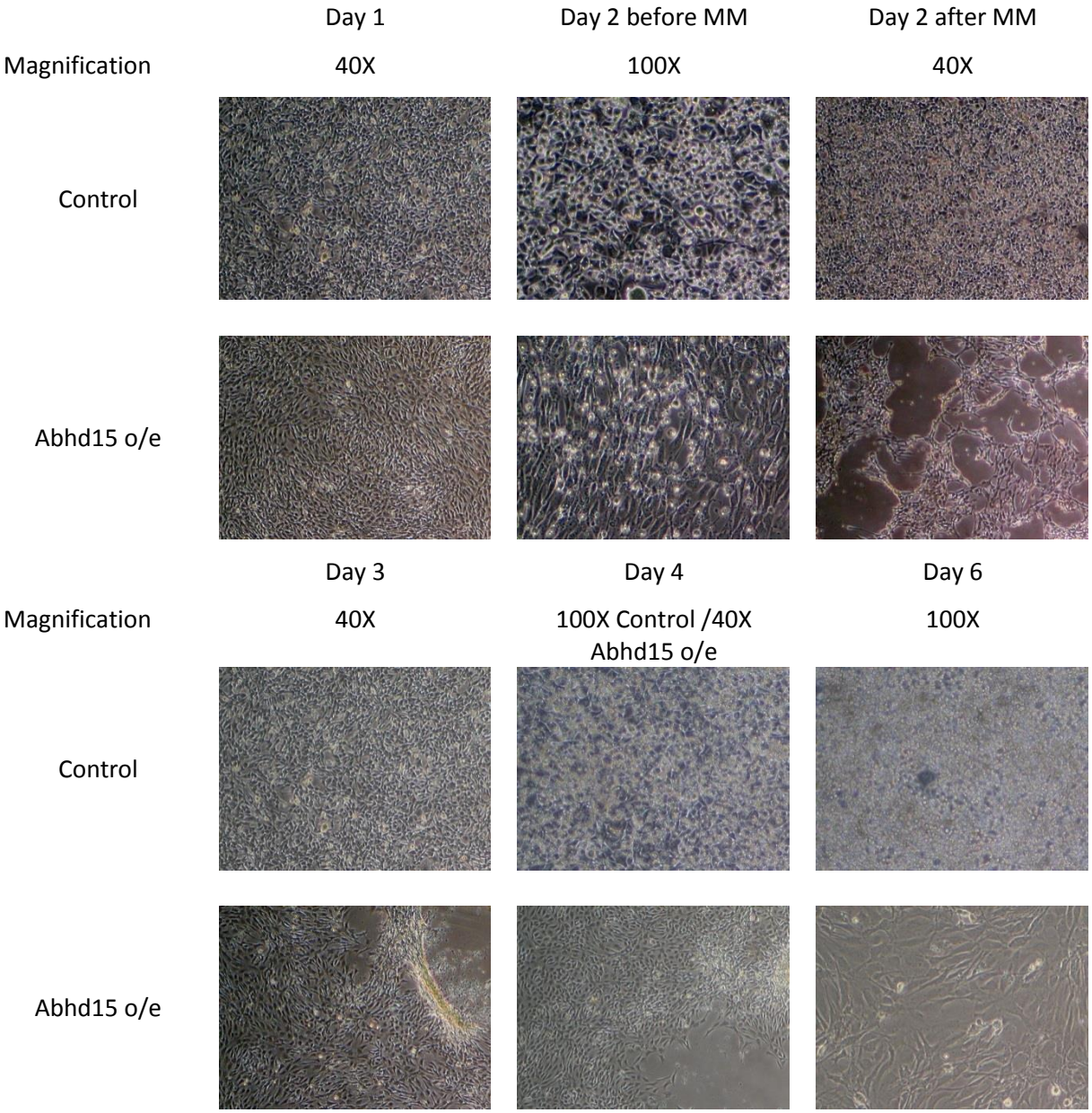

Figure 17: ***Differentiation of control and Abhd15 o/e iBACs.*** *Cells were differentiated from day 0 to day 6. Pictures show one representative passage (p24) out of 3 biological replicates. Days and the magnification of the microscope while taking the pictures are shown on top of the figure. MM stands for maintenance medium and indicates the medium change on day 2.*

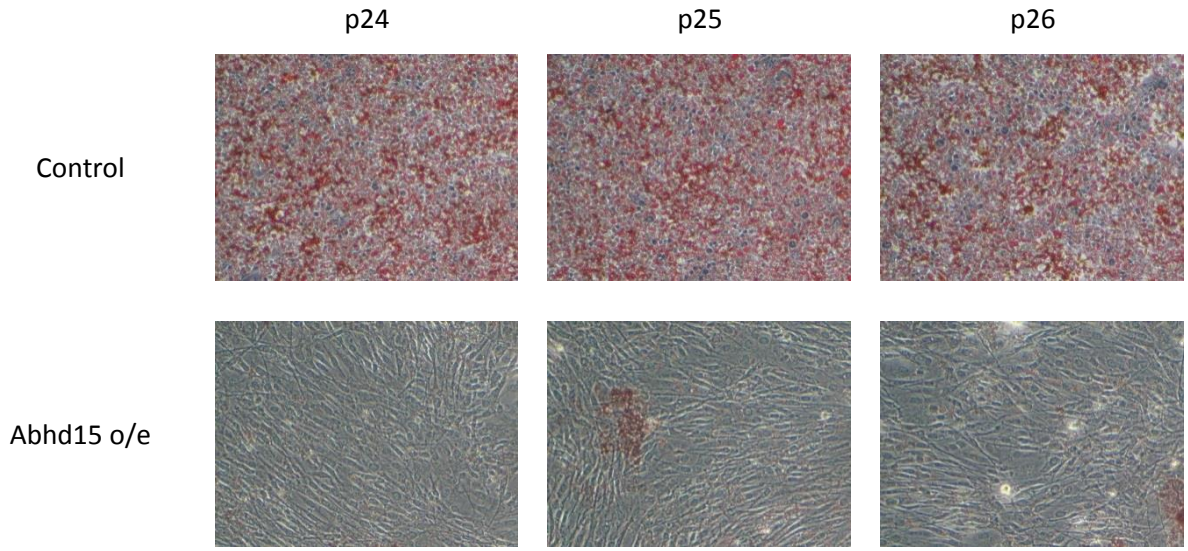

Figure 18: ***ORO staining of control and Abhd15 o/e iBACs at day 5 of differentiation****. The pictures show the three biological replicates (p24, p25 and p26) of Abhd15 o/e and control cells, magnified 100X.*

4.3.2 Proliferation of Abhd15 o/e iBACs

Proliferation assays showed that Abhd15 o/e iBACs proliferated slower than the control cells in the first 24 hours after seeding. In the following 2 time points (48 and 72 hours), there were no significant changes between the number of control and overexpressing cells (Figure 19). Only at the last time point, Abhd15 o/e cells proliferated faster. This can be seen by their increased cell number compared to the control cells after 96 hours (Figure 19).

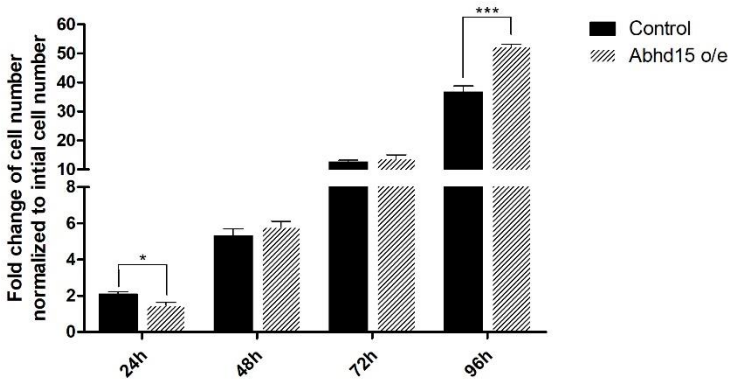

Figure 19: ***Cell proliferation assay of control and Abhd15 o/e iBACs.*** *Cells were counted after 24, 48, 72, and 96 hours. Results are represented as mean value ± sd, n = 3.*

4.3.3 Gene expression pattern of Abhd15 o/e iBACs

To investigate possible differences at mRNA levels during differentiation and to elucidate the possible cause of the differentiation defect, I harvested control and Abhd15 o/e cells at day 0, 2, 4, and 6 of differentiation. I took a closer look at browning markers including *Ucp1*, *Prdm16*, *Dio2,* and *cell death inducing DFFA like effector A* (*Cidea*). Further, I also checked the ß-oxidation marker *peroxisome proliferator activated receptor gamma coactivator 1α* (*Pgc1α*), which activates UCP1 expression and *Abhd15* to test the overexpression. Of note, this experiment has been performed twice and both attempts revealed similar results. One representative result is shown (Figures 20, 21).

Ucp1 (Ct-value = 28 compared to control Ct-value = 31,6) and *Dio2* (Ct-value = 28,9 compared to control Ct-value = 32) were strongly increased in Abhd15 o/e cells at day 2, whereas there was scarce any expression of *Prdm16* (Ct-value = 36,4 compared to control Ct-value = 31,9) during the whole differentiation process compared to the controls. Moreover, *Pgc1α* (Ct-value = 33 compared to control Ct-value = 26) was hardly determined and *Cidea* (Ct-value > 37 compared to control Ct-value = 31,1) was not detected in Abhd15 o/e cells. However, an increased expression of *Abhd15* could be observed almost every day (day 0: Ct-value = 23 compared to control Ct-value = 28,4) (Figures 20, 21).

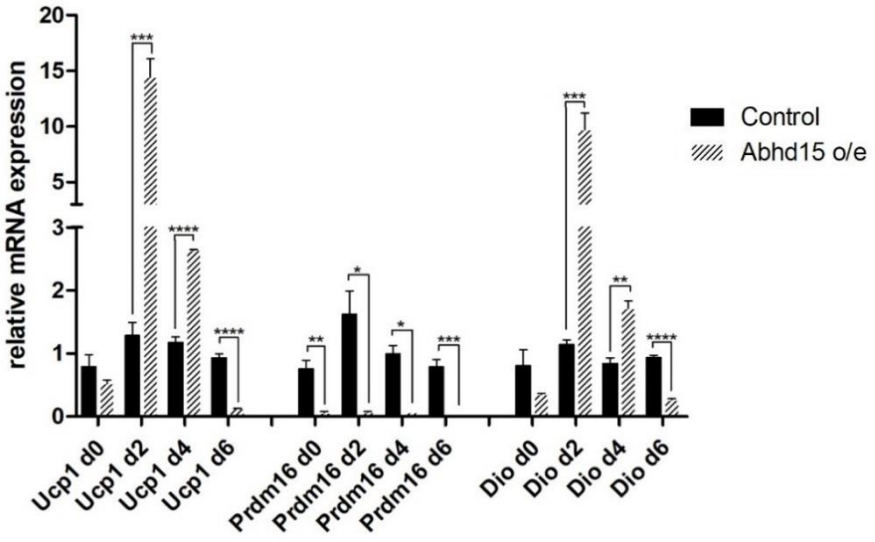

Figure 20: ***Browning genes in control and Abhd15 o/e iBACs.*** *mRNA expression during differentiation from day 0 to day 6 between control and Abhd15 o/e cells. Results are represented as mean value ± sd, n = 3.*

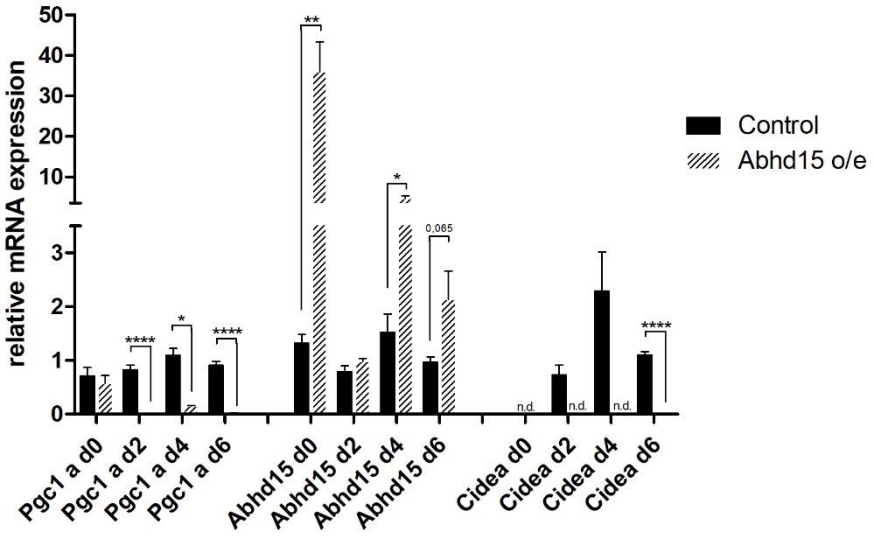

Figure 21: ***Browning genes in control and Abhd15 o/e iBACs.*** *mRNA expression during differentiation from day 0 to day 6 between control and Abhd15 o/e cells. Results are represented as mean value ± sd, n = 3.*

4.3.4 Protein expression pattern of ABHD15 o/e iBACs

To examine the protein expression pattern of Abhd15 o/e cells, 3 biological replicates of control and Abhd15 o/e cells were seeded in 6-well plates. After induction, I isolated proteins every 24 hours from day 0 until day 6. The isolated protein fractions were subjected to western blot analysis (Figures 22-24)

Interestingly, the overexpression of *Abhd15* achieved on mRNA levels (Figure 21) could not be observed at protein levels after two different attempts. Further, the expression levels of all detected proteins were lower in Abhd15 o/e compared to control cells (Figures 22, 23).

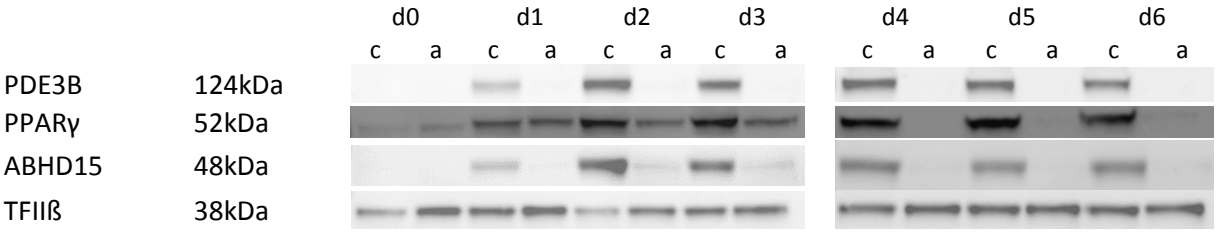

Figure 22: ***First western blot results of control and Abhd15 o/e iBACs.*** *Results show protein expression during differentiation from day 0 to day 6 between control and Abhd15 o/e cells. Whereas "c" stands for iBACs puro control cells and "a" for Abhd15 o/e iBACs. One biological replicate is shown.*

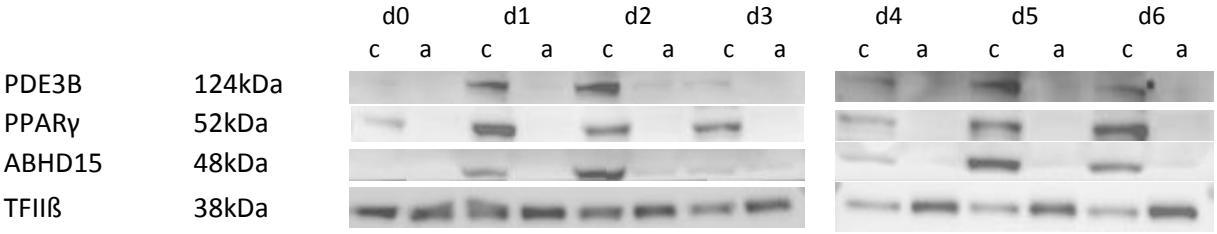

Figure 23: ***Second western blot results of control and Abhd15 o/e iBACs.*** *Results show protein expression during differentiation from day 0 to day 6 between control and Abhd15 o/e cells. Whereas "c" stands for iBACs puro control cells and "a" for Abhd15 o/e iBACs. One biological replicate is shown*

Since control cells showed a stronger protein signal than Abhd15 o/e cells, it was difficult to compare expression levels between them. Therefore, I repeated the western blot analysis on separated blots (Figures 24, 25).

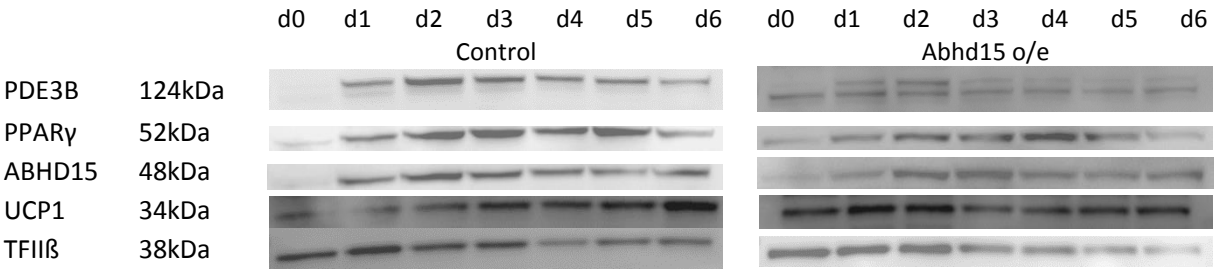

Figure 24: ***Western blot results of control and Abhd15 o/e iBACs on separated blots.*** *Results show differentiation from day 0 to day 6. On the left-hand side from control cells, on the right-hand side from Abhd15 o/e cells. One biological replicate is shown.*

Rising levels of ABHD15 during differentiation could be seen in control and Abhd15 o/e cells (Figure 25), whereas control cells showed a higher ABHD15 expression than the overexpressing cells. Even though UCP1 had similar expression on each day, one outlier could be seen on day 6 in the control cells where the expression was increased. PPARγ showed variations in protein levels from day 0 to day 6, with increased expression from day 2 until day 5 and lower expression on day 0 and day 6. PDE3B had the highest expression on day 2, with a declining drift from that day on (Figure 25).

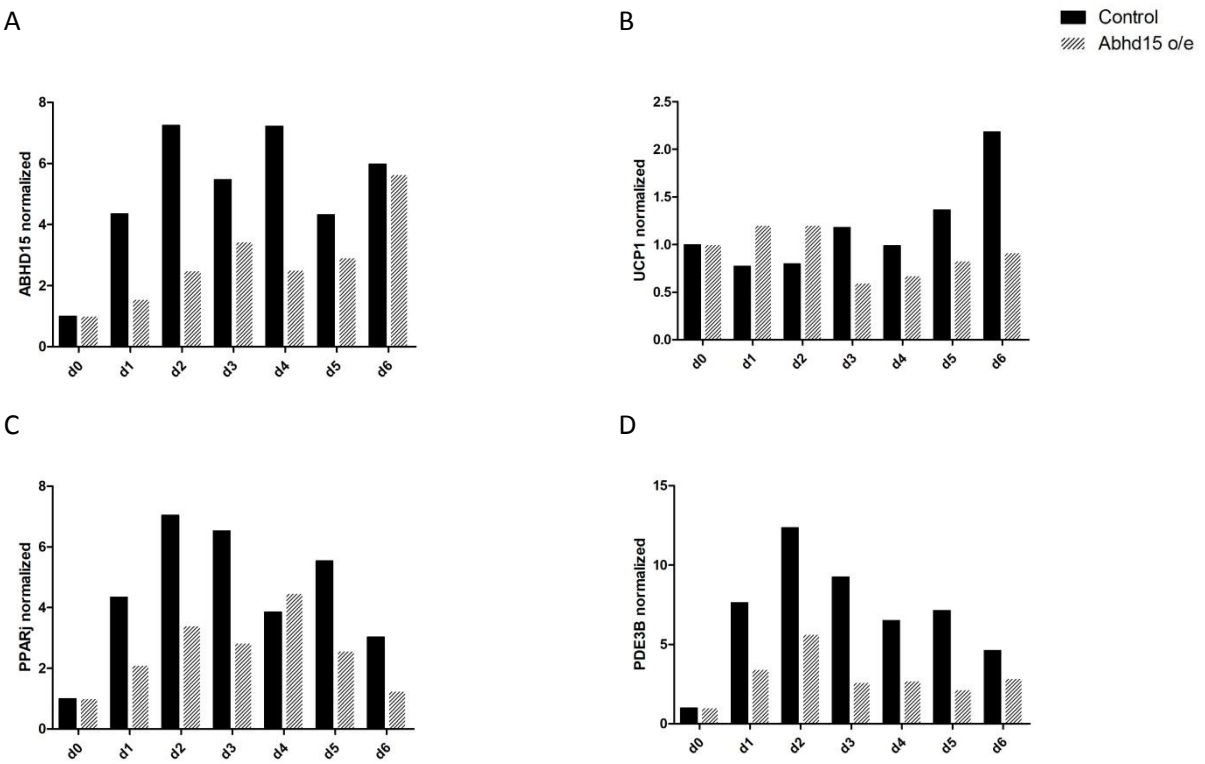

Figure 25: ***Quantification of protein expression from the separated blots****. Normalized protein of: A) ABHD15; B) UCP1; C) PPARγ; D) PDE3B. Results show the different protein levels from day 0 to day 6 during differentiation, between control and Abhd15 o/e iBACs. Each bar represents a single value.*

Due to time efficiency issues, the western blot membrane was cut after ponceauS staining and the separated parts were incubated with different primary antibodies. Since the ABHD15 bands were hardly detected in the cut membranes, I incubated the whole blot with the anti-ABHD15 primary antibody overnight. This could have indicated whether ABHD15 migrated with a different molecular weight than the expected due to, for instance, dimers formation.

According to the ABHD15 antibody manufacturer, the calculated molecular weight is 52 kDa, which corresponds with the observed molecular weight. However, western blot results performed in our laboratory showed that ABHD15 bands were around 48 kDa. The strongest band in the control cells could be seen between sizes of 39 and 51 kDa according to the protein standards (Figure 26).

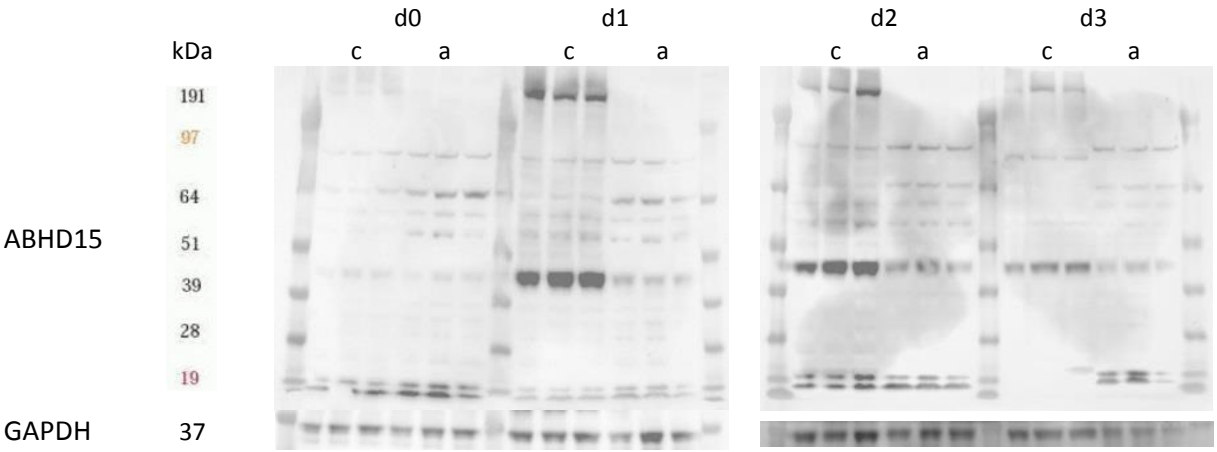

Figure 26: ***Whole membrane western blot results of control and Abhd15 o/e iBACs.*** *Protein expression during differentiation from day 0 to day 3 between control and Abhd15 o/e cells. Whereas "c" stands for iBACs puro control cells and "a" for iBACs Abhd15 o/e cells. Three biological replicates are presented.*

4.3.5 Endoplasmic reticulum stress and apoptosis in Abhd15 o/e iBACs

To further investigate the observed differentiation defect, I took a closer look at endoplasmic reticulum (ER) stress and apoptosis. PPARα is a marker for mitochondrial FA ß-oxidation. Moreover, studies showed Pparα as transcriptional suppressor, which leads to reduced ER stress and apoptosis of adipocytes [61]. *Pparα* was hardly expressed in Abhd15 o/e cells during differentiation (Figure 27). A*ctivating transcription factor 3* (*Atf3*), *activating transcription factor 4* (*Atf4*), *binding immunoglobulin protein* (*Bip*), and *transcription factor C/EBP homologous protein 10* (*Chop10*) are known to be upregulated under stress conditions [62], [63]. *Atf3*, *Atf4,* and *Chop* showed reduced expression levels compared to controls. *Bip* also showed lower levels than control cells, with the exception of day 3 with 36b4 as housekeeping, where it was increased (Figure 27).

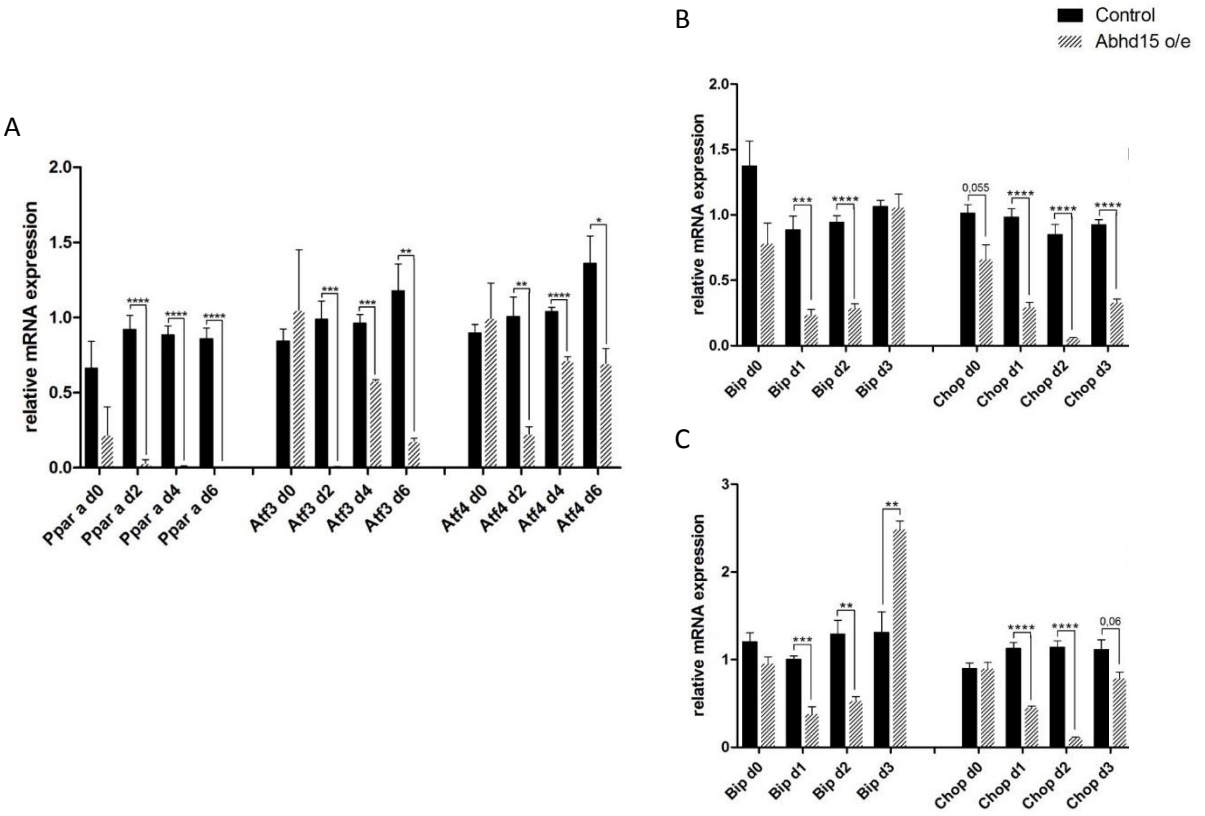

Figure 27: ***ER-stress markers expressions.*** *mRNA expression was measured from day 0 to day 3 of differentiation between control and Abhd15 o/e cells. A) Atf3, and Atf4 with Tfiiß as housekeeping gene; B) Bip, Chop with Tfiiß as housekeeping gene; C) Bip, Chop with 36b4 as housekeeping gene. Results are represented as mean value ± sd, n = 3.*

Next, I checked apoptosis by analyzing the expression of the apoptotic marker cleaved caspase 3 (CC3). However, no significant difference could be observed between control and Abhd15 o/e iBACs (Figure 28).

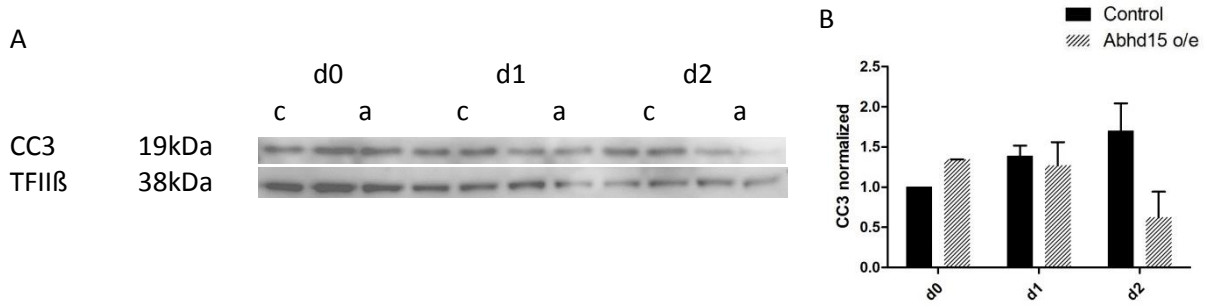

Figure 28: ***CC3 expression in control and Abhd15 o/e iBACs.*** *A) Western blot of CC3 expression at days 0, 1 and 2 of differentiation in control and Abhd15 o/e cells; B) Western blot quantification of CC3. Whereas "c" stands for control cells and "a" for Abhd15 o/e cells. Results are represented as mean value ± sd, n = 1-2*

4.4 Transient overexpression of Abhd15 in iBACs

To confirm the data from the experiments performed with the cell line that was available in our laboratory, I generated a new batch of Abhd15 o/e cells. Transfection and transduction were performed as described in the methods. First, I checked whether there was a differentiation defect as observed in the previous experiments. However, a defect was not observed in this batch of Abhd15 transduced cells (Figure 29). The most efficient transduction yield was achieved by infecting the cells at day 0, when they reached about 95% cell confluence and a second time during differentiation at day 2.

Since results represent only one sample, no statistical significance was calculated. Nevertheless, *Abhd15* expression was increased by 2,5-fold in transduced cells compared to controls (Figure 30). That means, the fold change of *Abhd15* between the overexpression and the transduction cells was nearly the same, at least at day 6 (Figures 21, 30). The other genes were hardly expressed in the Abhd15 o/e cells compared to their controls at day 6 of differentiation (Figures 20, 21). Transduced cells, however, did not show the same low expressed gene levels compared to their control cells (Figure 30).

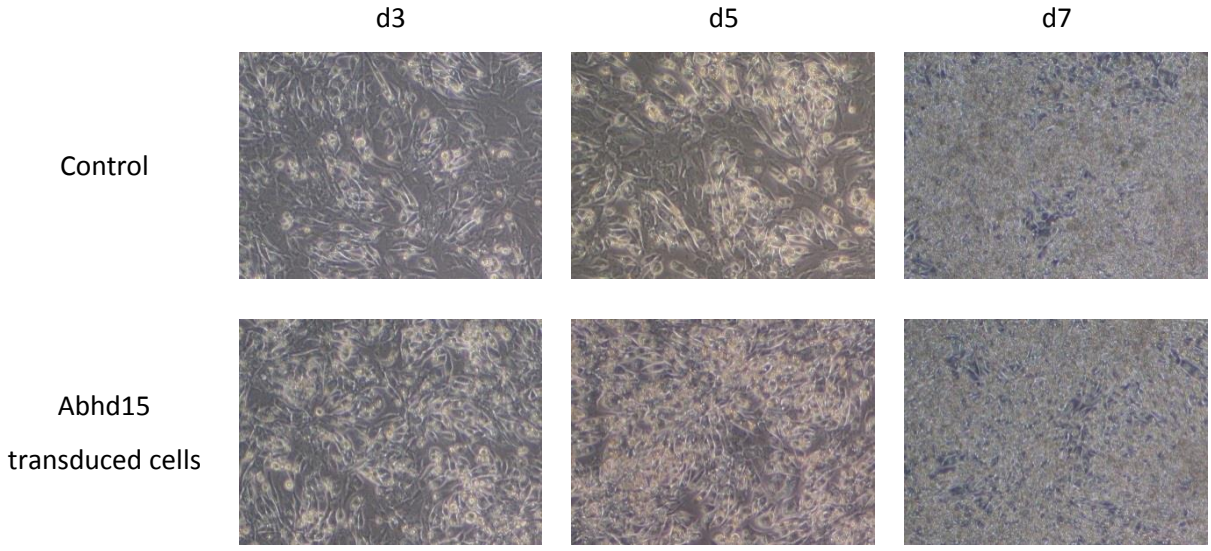

Figure 29: ***Differentiation of transduced control and Abhd15 cells:*** *Cells were differentiated from day 0 to day 7. Pictures show representative days from one passage between control and Abhd15-transduced cells, with 100X magnification.*

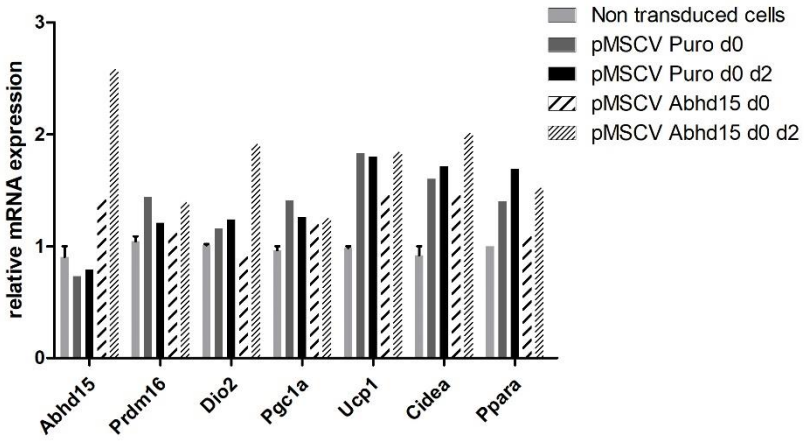

Figure 30: ***Browning genes in transduced control and Abhd15 cells.*** *mRNA expression levels on day 6 of differentiation. Results are represented as mean value ± sd, for n = 2 or as single value for n = 1.*

In contrast to the Abhd15 o/e cells (Figures 22, 23), the transduced cells did not show the same reduced protein levels (PDE3B, PPARγ, ABHD15) in differentiated adipocytes (Figure 31). The numbers indicate different conditions (Table 6). Cells transduced at 95% confluence and directly induced for differentiation showed slightly higher ABHD15 levels than control cells (condition 1 and 2, Figure 31). Cells transduced at 40% confluence showed reduced ABHD15 levels compared to controls (condition 3 and 4, Figure 31).

Table 6: Setting of the cell confluence and number of transduction

	Days of transduction			
Condition	1	2	3	4
Cell confluency	95 %	95 %	40 %	40 %
pMSCV Puro	d0	d0, d2	d0	d0, d2
pMSCV Abhd15	d0	d0, d2	d0	d0, d2

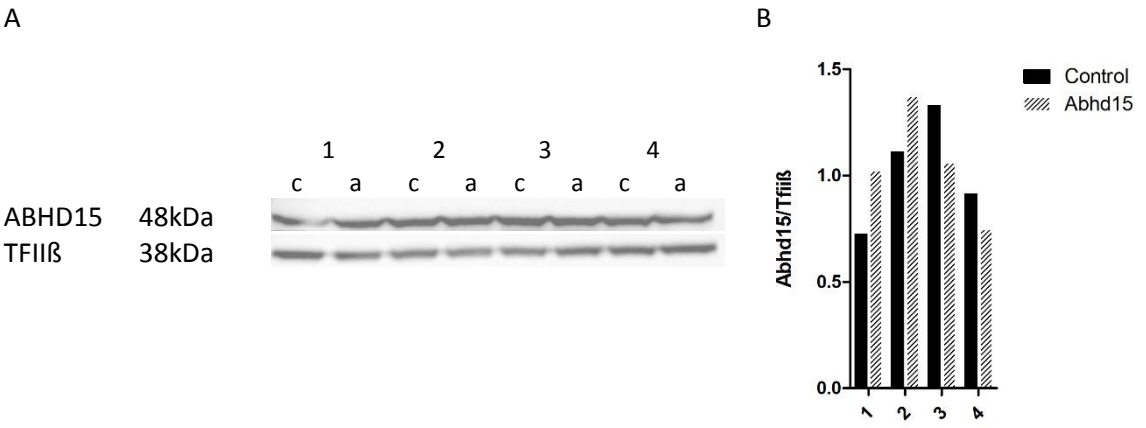

Figure 31: ***Western blot results of transduced control and Abhd15 cells.*** *A) ABHD15 expression at day 7 of differentiation. Whereas "c" stands for control cells and "a" for Abhd15 o/e cells. Numbers indicate each condition (Table 6). B) Western blot quantification, the bars represent single values.*

4.5 Electroporation of pMSCV or pMSCV-Abhd15 in iBACs

As it has been shown in the preceding section, the gene expression levels reached after the transduction of the iBACs with pMSCV-Abhd15 vector were not promising in terms of the overexpression (*Abhd15* Ct-value = 23,4 compared to control Ct-value = 24,9). Therefore, with the aim to reach higher expression levels, I performed electroporation of the pMSCV-Abhd15 and empty vectors, as described in the methods section. Unfortunately, it was not possible with this method to achieve a strong overexpressing cell line for further analysis (Figure 32).

A

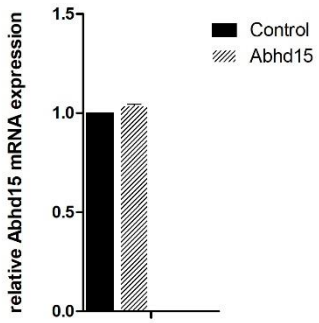

B

Sample	target	CT-value	Ratio
Control, d5, c=0,25	*Abhd15*	26,47	1,00
	TfIIb	28,54	
iBacs Abhd 1, d5, c=0,25	*Abhd15*	27,90	1,05
	TfIIb	29,92	
iBacs Abhd 2, d5, c=0,25	*Abhd15*	26,88	1,03
	TfIIb	28,91	

Figure 32: ***Electroporation of pMSCV or pMSCV-Abhd15.*** *A) Relative Abhd15 mRNA expression in cells electroporated with pMSCV or pMSCV-Abhd15; B) CT values of Abhd15 and TfIIβ as housekeeping gene after 5 days of differentiation. Abhd15 expression is presented as the ratio between the two groups.*

4.6 Regulation of ABHD15 in murine BAT

4.6.1 ABHD15-KO reduces PDE3B expression in BAT

To investigate whether ABHD15 has an effect on PDE3B expression in BAT, I harvested tissues from WT and Abhd15-KO mice. Subsequently, BAT was homogenized, protein was isolated and subjected to western blot analysis. As shown, PDE3B levels in BAT from Abhd15-KO mice were decreased compared to their WT littermates (Figure 33).

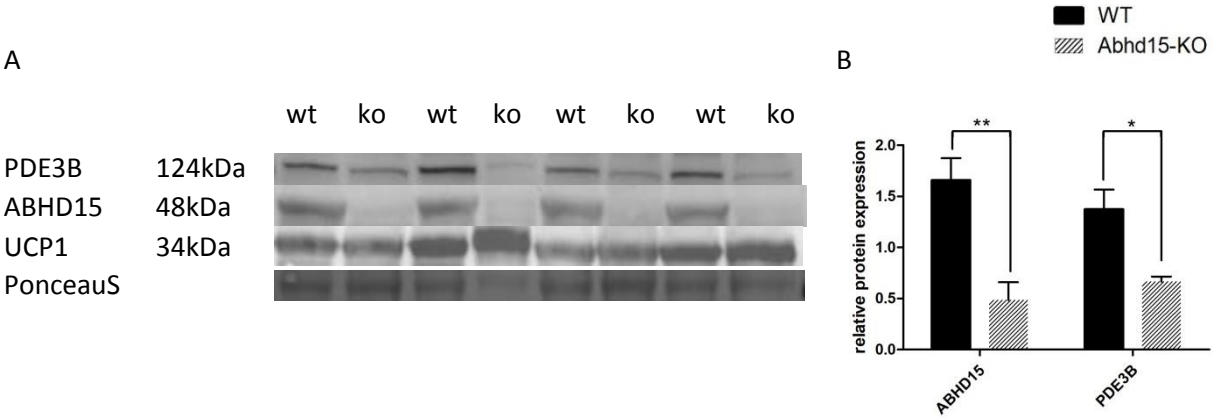

Figure 33: ***PDE3B and ABHD15 expression in BAT from WT and Abhd15-KO mice.*** *A) Western blot of PDE3b and ABHD15 in WT compared to Abhd15-KO mice; B) Western blot quantification, results are represented as mean value ± sd, n = 4.*

4.6.2 Regulation of ABHD15 and PDE3B by cold exposure

Next, we investigated the regulation of ABHD15 and PDE3B in BAT in response to cold exposure. Thus, we set WT mice at room temperature (RT) or at 4°C for 24 hours or 3 weeks. Interestingly, reduced levels of ABHD15 and PDE3B were detected after 24 hours and significantly reduced levels after 3 weeks of cold exposure (Figure 34).

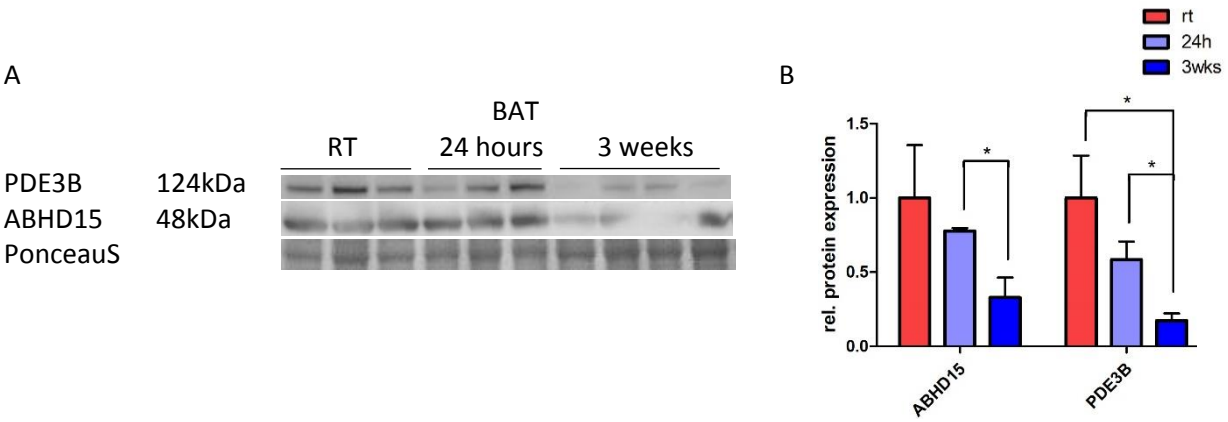

Figure 34: ***Effect of cold exposure on PDE3B and Abhd15 expression in BAT.*** *A) PDE3B and ABHD15 expression levels in BAT from WT mice kept at room temperature (RT) or after 24 hours or 3 weeks under cold exposure; B) Quantification from the Western blot performed with BAT samples Results are represented as mean value ± sd, n = 3-4.*

4.6.3 ABHD15 expression in BAT under different nutritional states

The Bogner-Strauss laboratory showed that ABHD15 is downregulated upon overnight fasting and upregulated after 1 and 2 hours of refeeding in WAT at mRNA and protein levels, at least in lean and healthy mice [22], [28]. Therefore, I investigated whether the same effect occurs in BAT. In contrast to WAT, ABHD15 and PDE3B expression levels were both lower after 2 hours of refeeding compared to 1 hour of refeeding (Figure 35). Due to insufficient samples in terms of volume and amount of replicates, this experiment could not be repeated. Thus, the regulation of ABHD15 and PDE3B due to 1 and 2 hours of refeeding in BAT could not be fully clarified.

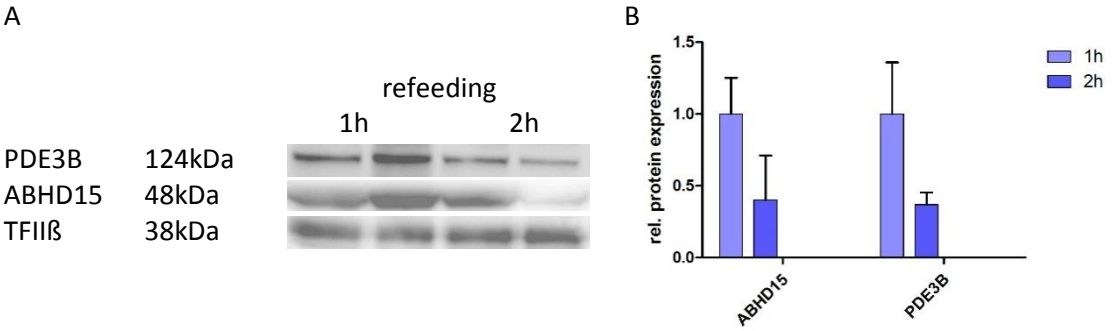

Figure 35: ***Western blot results and quantification of BAT at different nutritional states.*** *A) Protein expression of mice after overnight fasting and 1 to 2 hours of refeeding; B) Protein quantification, results are represented as mean value ± sd, n = 2.*

4.6.4 Dietary effect on ABHD15 expression

Abhd15 mRNA expression has been previously shown to be reduced in WAT from mice fed with HFD in comparison to CD [28]. In BAT, my results showed that ABHD15 levels did not change between mice fed a HFD and CD, while I detected a significant increase in ABHD15 protein expression in mice fed with HGD compared to controls (Figure 36).

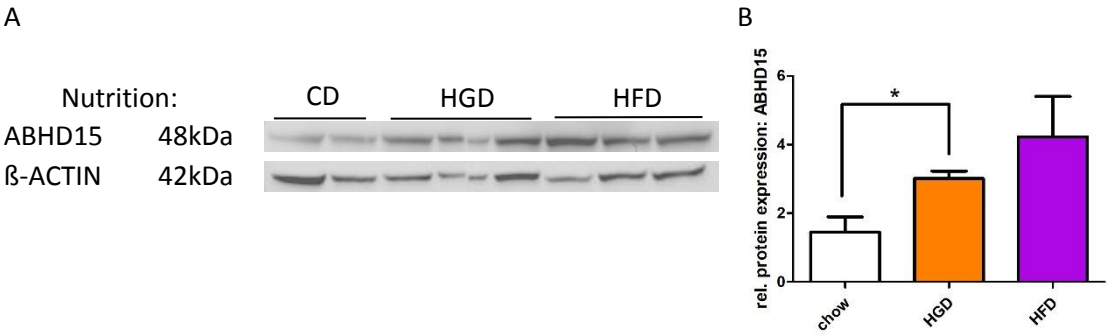

Figure 36: ***Dietary effects on ABHD15 expression in BAT.*** *A) ABHD15 expression in BAT from mice fed with chow diet (CD), high glucose diet (HGD) or high-fat diet (HFD); B) Western blot quantification. Results are represented as mean value ± sd, n = 2-3.*

5 Discussion

5.1 Microarray experiment

The microarray experiment was performed as an initial approach to elucidate the potential role of ABHD15 in BAT. Interestingly, several genes were dysregulated between Abhd15-KO and WT mice. However, we faced some unexpected troubles regarding the genotyping of the mice included in this experiment. One mouse initially included as WT turned out to be Abhd15-KO. Thus, we finally ended up with only 3 WT and 5 Abhd15-KO animals. An experimental design of 4 vs 4 as originally planned would have yielded in a more significant outcome and a higher number of DEGs. After an intense literature search, only one direct relation amongst the closer investigated DEGs and BAT has been found (Tables 3, 4).

Microarray technologies have the benefit to examine the expression of thousands of genes at the same time with several limitations such as accuracy, precision, and specificity [64]. For the initial screening purposes used in this thesis, these limitations are less relevant. Although the technologies have considerably improved over the last years and it became a powerful research tool, the validation of the microarray data by other gene expression techniques is recommended [64], [65].

The significant differences at gene expression levels between WT and KO mice from the microarray experiment were not reproducible by qPCR in the validation part of the study (Figure 10). Even though the same samples were used, many factors such as the above mentioned microarray limitations could have influenced the different outcomes. Other explanations are the pitfalls concerning the qPCR like mispriming or the creation of primer dimers, the exponential amplification of errors, or the variation of efficiency at later cycles. For the microarray analysis non-specific or cross hybridizations can occur [66].

The disparity with the results from the independent mouse experiment could be due to the differences between the first and the second cohort in terms of age and nutrition.

5.2 Gene set enrichment analysis

5.2.1 Hydrogen peroxide metabolic process

Hydrogen peroxide (H_2O_2) is a capable noxious byproduct in many chemical reactions, such as the aerobic cellular respiration in mitochondria [45] [46]. Recent studies in mouse models as well as in isolated brown adipocytes showed increased levels of mitochondrial hydrogen peroxide during the activation of BAT thermogenesis [46].

5.2.2 Regulation of energy homeostasis

BAT has an important role to maintain the body core temperature, especially in cold surroundings, burning energy for thermogenesis. Further, it possesses the ability to consume energy excess [48], [49]. The oxygen consumption in BAT could nearly double in rats which had adapted to cold exposure, compared to the oxygen consumption during thermoneutrality [48]. At least in mice, it could be shown that BAT is an effective player against diet-induced obesity [48]. Moreover, BAT holds the ability not only to use energy from lipid storage, but also from glucose and circulating TGs [49]. Summing up all the mentioned points above, BAT become a possibly player in the treatment against obesity in human, however further research is needed in this direction [48].

5.2.3 Thyroid hormone metabolic process

Physiologically increased thyroid hormone levels result in higher lipolysis and gluconeogenesis, raised resting energy expenditure, and weight reduction [52]. AT is an important target of the thyroid hormones, which are required for many processes taking place in the AT like lipolysis, lipogenesis, thermogenesis, mitochondrial function, and accessibility of nutrients by regulating key genes [53]. Especially due to the elevated expression of *Dio2* in BAT and its activation of T3, this pathway plays a main role in brown adipogenesis and thyroid-hormone-dependent thermogenic pathways, responsible of UCP1 and PGC1a expression [54]. Hence, adipogenesis in BAT leads to a higher thermogenic performance, represented as increased UCP1 levels [53]. Thus, thyroid-hormone signaling speeds up energy expenditure and stands in an essential relation to BAT, by insuring functionality and brown adipogenesis, in animal and cell models [54].

5.2.4 Regulation of superoxide metabolic pathway

One example, in which O_2^- could emerge inside of cells, is spontaneous autoxidation through redox enzymes, where O_2 gets reduced to O_2^-. O_2^- is subsequently further reduced to a hydroxyl radical, which leads to DNA damage. Preventing the cells from damage, the superoxide dismutase keeps the O_2^- at a manageable concentration [56]. In BAT, reactive oxygen species are primarily generated by mitochondria. Electrons, which escape the respiratory chain, reduce the oxygen to O_2^-. It has been showed, that during FA oxidation and after cold exposure, UCP1 has the ability to decrease O_2^- generation enabling a high oxidative capacity exclusive of oxidative damage [57].

5.2.5 Negative and positive regulation of steroid metabolic process

AT accumulation differs in localization concerning to sex and gender. Common female depots develop predominantly peripheral and lower, whereas male fat depots are located more central and visceral. This differences in fat distribution are due to interactions of steroid sex hormones with AT [59]. Steroid hormones act on AT over specific receptors expressed in BAT and WAT [59], [60]. During the period of childbearing and lactation, an increased sex hormone level in women is associated with BAT reduction. This reduction is represented by suppressed thermogenesis, using the saved energy for fetal development [60]. In addition, positron emission tomography studies revealed that apparently active BAT is twice that frequent in women than in men. Still, it is controversially discussed, if sex differences in BAT physiology truly exist. One possible explanation could be the higher sensitivity of women against cold. More convincing were the outcomes in rodent experiments. Male mice showed lower amounts of interscapular BAT, proportional to their body weight, in comparison to their female counterparts. Further, a faster reduction of UCP1 with increased age could be observed [59].

In contrast to DEGs, biological processes including energy homeostasis, reactive oxygen species and hormone metabolism, could all be related to BAT function (Table 5). Additionally, the number of dysregulated genes in Abhd15-deficient BAT of the above mentioned pathways indicate potential interesting functions of ABHD15 (Figures 11 to 16). However, further research is necessary to elucidate the exact role of ABHD15 in such processes.

5.3 Abhd15 o/e iBACs already available in the lab

Overexpressing or silencing a gene of interest in cell lines or animal models comprise a widely used approach to study its effect/s in specific molecular pathways. In this case, the second part of my thesis was carried out using either Abhd15 o/e iBACs or BAT samples from Abhd15-KO mice, which were already available in our laboratory.

Initially, we induced Abhd15 o/e cells and their respective controls to adipocyte differentiation. During this process, Abhd15 o/e cells detached and died, leaving cell gaps on well plate surfaces (Figure 17). In contrast, control cells were differentiated from brown preadipocytes into mature brown adipocytes without any unexpected effect. When I observed this fact for the first time, I thought of a possible contamination, a general mistake due to wrong cell handling or incorrect preparation of the medium. After a negative mycoplasm test and re-checking the experimental setup, subsequent attempts led to the same results. Since control cells were always successfully differentiated, we excluded incorrect handling or problems related to the experimental setup as causes of the differentiation defect. It is likely that this phenotype is inherent to Abhd15 o/e cells.

mRNA expression analyses showed that *Ucp1, Dio2* and *Prdm16* levels were decreased at day 0. This indicated a reduced browning phenotype of the overexpressing cells, while *Abhd15* mRNA expression itself was successfully increased (Figure 21). During the whole differentiation process, *Prdm16*, *Cidea* and *Pgc1α* were highly reduced in Abhd15 o/e in contrast to control cells (Figures 20, 21). On the other hand, it was not possible to show any ABHD15 overexpression of the Abhd15 o/e cell line at protein levels (Figures 22, 23). Further, all detected proteins seemed to be strongly decreased in the overexpressing compared to the control cells.

Additionally, control and Abhd15 o/e samples from day 0 to 3 showed bands distributed over the entire membrane and not just at the expected 48 kDa (Figure 26). There are different reasons for the detection of bands with lower and higher molecular weights than expected. Technical causes for lower molecular weight bands can be degradation of the protein by insufficient cooling during handling the samples or repeatedly freeze and thaw cycles. Other reasons for lower bands could be through splicing or cleavage into additional forms of the protein. NCBI protein BLAST for example showed that an unnamed protein

product in mice has a query cover of 92% compared to ABHD15. Bands with higher molecular weight than the expected may occur on account of unresolved protein multimers or proteins which bind to modifiers. I observed some bands with higher intensity in the Abhd15 o/e than in the control cells, especially in the upper membrane area (Figure 26). This could be a hint for dimer formation and maybe one reason for hardly any ABHD15 protein expression, while there is a clear overexpression at mRNA levels. However, this still did not clarify the overall lower protein levels of the detected proteins in Abhd15 o/e compared to the control cells.

Therefore, I tested apoptosis CC3 as a widely recognized proapoptotic marker [67] in Abhd15 o/e cells. However, I did not observe increased CC3 protein levels in Abhd15 o/e cells (Figure 28). Since I was not able to find a potential relation between the observed differentiation defect and apoptosis, I next investigated ER stress as another potential cause of this finding.

Disturbances in the ER equilibrium affect protein folding and can lead to ER stress [62]. In response, ER chaperone mechanisms get upregulated and, consequently, unfolded protein response is activated. If ER stress excels the chaperone mechanisms, the organelle transmits apoptotic signals. One important player of this stress-mediated apoptosis pathway is CHOP, whereas BIP belongs to the ER chaperone proteins and is upregulated through the ER stress response pathway. BIP dissociates from the stress sensors PERK, IRE1 and ATF6 via binding to unfolded proteins and thereby activates their signaling pathway. From this three stress sensors, the PERK pathway plays a main role in CHOP induction as response to ER stress [62]. I therefore took a closer look on the PERK pathway. This pathway includes the alpha subunit of the eukaryotic initiation factor 2 (eIF2α), ATF3, ATF4, and CHOP. After the activation of the PERK pathway through BIP, PERK subsequently phosphorylates eIF2α. ElF2α further activates ATF4, which targets CHOP and thereby induces apoptosis. ATF3 may also participate in the regulating of CHOP expression, as it is reported that ATF3 is increased under certain ER-stress situations [62], [63]. BIP mRNA expression was significantly downregulated in Abhd15 o/e iBACs at day 1 and 2 of differentiation, which did not indicate any activation of ER chaperone mechanism in response to ER stress (Figure 27). Further, associated with the PERK pathway, no increased expression of ATF3, ATF4 and CHOP itself could be observed in Abhd15 o/e cells. Thus, a connection between the differentiation defect and an increased ER-stress inducing apoptosis still remains elusive.

The attempt to establish a new Abhd15 o/e iBACs line was unfortunately not fruitful and investigations concerning the possible role of ABHD15 on a cellular basis could not be performed (Figures 30, 32).

5.4 Regulation of Abhd15 in murine BAT

5.4.1 ABHD15-KO reduces PDE3B expression in BAT

When nutrients are metabolized into glucose, the insulin signaling pathway is activated to ensure energy uptake by insulin target cells. As a consequence, PDE3B levels are increased and AT lipolysis is suppressed. In contrary, during fasting PDE3B levels are decreased and lipolysis is active [22].

In WAT, ABHD15 stabilizes PDE3B and influences its expression. WAT-specific Abhd15-KO mice showed reduced expression of PDE3B and induced an unrestrained FA mobilization. This is further accompanied by a glucose uptake, which promotes insulin resistance [22]. Results in BAT displayed reduced PDE3B protein levels in whole-body Abhd15-KO mice (Figure 33), suggesting a similar effect of ABHD15 on PDE3B expression in BAT. Hence, ABHD15 deficiency could evocate insulin resistance in BAT as well as it has been described for WAT. However, to confirm this hypothesis, similar experiments as performed in WAT need to be performed in BAT, including determination of plasma lipid parameters like TGs and FAs. Further, insulin and glucose tolerance tests should be performed. The assignments for this task would excel the frame of this master thesis.

5.4.2 Reaction of cold exposure in murine BAT

Studies carried out in rodents and humans denoted that cold exposure of BAT leads to increased levels of *Ucp1*/UCP1 on mRNA and protein level [10]. Moreover, the cold exposure experiments performed during this thesis showed a significant decrease of ABHD15 and PDE3B in BAT (Figure 34). One explanation could be the higher energy consumption, expended by thermogenesis to maintain the body temperature in cold surroundings. This elevated energy is provided by reduction of PDE3B levels. Consequently, lipolysis is activated, and stored energy is released in form of FAs. A next step could be to measure body weight during cold exposure to elucidate potential body weight loss differences between BAT-specific Abhd15-KO and control mice exposed to cold. Regarding the reported function of altering PDE3B stability by ABHD15, I observed that PDE3B and ABHD15 protein level were similarly expressed, conforming the stabilizing role mentioned above (Figure 34).

In conclusion, this thesis set the initial basis for further investigations aiming to draw a clearer picture regarding the role of ABHD15 in BAT. First, a working overexpression or silenced brown adipocyte cell line would be interesting to enlighten the role of Abhd15 on a cellular basis. Moreover, studies comparing the metabolic phenotype of whole-body Abhd15-KO with BAT-specific Abhd15-KO mice comprise, to my opinion, a very interesting approach for the future.

6 References

[1] "Obesity and overweight." [Online]. Available: http://www.who.int/mediacentre/factsheets/fs311/en/.

[2] J. M. Rutkowski, J. H. Stern, and P. E. Scherer, "The cell biology of fat expansion," *Journal of Cell Biology*, vol. 208, no. 5. pp. 501–512, 2015.

[3] A. Bartelt and J. Heeren, "Adipose tissue browning and metabolic health," *Nature Reviews Endocrinology*, vol. 10, no. 1. pp. 24–36, 2014.

[4] E. D. Rosen and B. M. Spiegelman, "What we talk about when we talk about fat," *Cell*, vol. 156, no. 1–2, pp. 20–44, 2014.

[5] S. S. Choe, J. Y. Huh, I. J. Hwang, J. B. J. I. Kim, and J. B. J. I. Kim, "Adipose tissue remodeling: Its role in energy metabolism and metabolic disorders," *Front. Endocrinol. (Lausanne).*, vol. 7, no. APR, pp. 1–16, 2016.

[6] A. Armani *et al.*, "Cellular models for understanding adipogenesis, adipose dysfunction, and obesity," *Journal of Cellular Biochemistry*, vol. 110, no. 3. pp. 564–572, 2010.

[7] V. Peirce, S. Carobbio, and A. Vidal-Puig, "The different shades of fat," *Nature*, vol. 510, no. 7503. pp. 76–83, 2014.

[8] F. W. Kiefer, "Browning and thermogenic programing of adipose tissue," *Best Practice and Research: Clinical Endocrinology and Metabolism*, vol. 30, no. 4. pp. 479–485, 2016.

[9] L. D. A. Brondani, T. S. Assmann, G. C. K. Duarte, J. L. Gross, L. H. Canani, and D. Crispim, "The role of the uncoupling protein 1 (UCP1) on the development of obesity and type 2 diabetes mellitus.," *Arq. Bras. Endocrinol. Metabol.*, vol. 56, no. 4, pp. 215–225, 2012.

[10] D. T. Chu and B. Gawronska-Kozak, "Brown and brite adipocytes: Same function, but different origin and response," *Biochimie*, vol. 138. pp. 102–105, 2017.

[11] K. Sarjeant and J. M. Stephens, "Adipogenesis," *Cold Spring Harb. Perspect. Biol.*, vol. 4, no. 9, pp. 1–19, 2012.

[12] J. Nedergaard, T. Bengtsson, and B. Cannon, "Unexpected evidence for

active brown adipose tissue in adult humans.," *Am. J. Physiol. Endocrinol. Metab.*, vol. 293, no. 2, pp. E444-52, 2007.

[13] M. Esteve Ràfols, "Adipose tissue: Cell heterogeneity and functional diversity," *Endocrinol. y Nutr. (English Ed.*, vol. 61, no. 2, pp. 100–112, 2014.

[14] M. Borga *et al.*, "Brown adipose tissue in humans: Detection and functional analysis using PET (positron emission tomography), MRI (magnetic resonance imaging), and DECT (dual energy computed tomography)," *Methods Enzymol.*, vol. 537, pp. 141–159, 2014.

[15] E. D. Rosen, C. J. Walkey, P. Puigserver, and B. M. Spiegelman, "Transcriptional regulation of adipogenesis Transcriptional regulation of adipogenesis," *Genes Dev.*, vol. 14, no. Rosen, E. D., Walkey, C. J., Puigserver, P., Spiegelman, B. M. (2000). Transcriptional regulation of adipogenesis Transcriptional regulation of adipogenesis. Genes & Development, 14, 1293–1307. http://doi.org/10.1101/gad.14.11.1293, pp. 1293–1307, 2000.

[16] F. M. GREGOIRE, C. M. SMAS, and H. S. SUL, "Understanding Adipocyte Differentiation," *Physiol. Rev.*, vol. 78, no. 3, pp. 783–809, 1998.

[17] E. D. Rosen and O. A. MacDougald, "Adipocyte differentiation from the inside out," *Nature Reviews Molecular Cell Biology*, vol. 7, no. 12. pp. 885–896, 2006.

[18] E. C. Lowe, S. O'Rahilly, and J. J. Rochford, "Adipogenesis at a glance," *J. Cell Sci.*, 2011.

[19] M. A. Lazar, "Becoming fat.," *Genes Dev.*, vol. 16, no. 1, pp. 1–5, 2002.

[20] R. Zechner, P. C. Kienesberger, G. Haemmerle, R. Zimmermann, and A. Lass, "Adipose triglyceride lipase and the lipolytic catabolism of cellular fat stores," *J. Lipid Res.*, vol. 50, no. 1, pp. 3–21, 2009.

[21] N. A. Ducharme and P. E. Bickel, "Minireview: Lipid droplets in lipogenesis and lipolysis," *Endocrinology*, vol. 149, no. 3, pp. 942–949, 2008.

[22] W. Xia *et al.*, "Loss of ABHD15 Impairs the Anti-lipolytic Action of Insulin by Altering PDE3B Stability and Contributes to Insulin Resistance," *Cell Rep.*, vol. 23, no. 7, pp. 1948–1961, 2018.

[23] C. C. Lord, G. Thomas, and J. M. Brown, "Mammalian alpha beta hydrolase

domain (ABHD) proteins: Lipid metabolizing enzymes at the interface of cell signaling and energy metabolism," *Biochim. Biophys. Acta - Mol. Cell Biol. Lipids*, vol. 1831, no. 4, pp. 792–802, 2013.

[24] "NCBI hAbhd15 gene." [Online]. Available: https://www.ncbi.nlm.nih.gov/gene/116236.

[25] "UniProtKB hAbhd15 protein." [Online]. Available: http://www.uniprot.org/uniprot/Q6UXT9.

[26] "NCBI mAbhd15 gene." [Online]. Available: https://www.ncbi.nlm.nih.gov/gene/67477.

[27] "UniProtKB mAbhd15 protein." [Online]. Available: http://www.uniprot.org/uniprot/Q5F2F2.

[28] E. Walenta *et al.*, "α/β-hydrolase domain containing protein 15 (abhd15) - An adipogenic protein protecting from apoptosis," *PLoS One*, vol. 8, no. 11, pp. 1–11, 2013.

[29] A. Subramanian, P. Tamayo, V. K. Mootha, S. Mukherjee, and B. L. Ebert, "Gene set enrichment analysis : A knowledge-based approach for interpreting genome-wide," 2005.

[30] K.-F. E. Vamsi K Mootha, Cecilia M Lindgren, "PGC-1α-responsive genes involved in oxidative phosphorylation are coordinately downregulated in human diabetes," *Nat. Genet.*, 2003.

[31] "PCR." [Online]. Available: http://www.enzolifesciences.com/science-center/technotes/2017/march/what-are-the-differences-between-pcr-rt-pcr-qpcr-and-rt-qpcr?/.

[32] F. Ponchel *et al.*, "Real-time PCR based on SYBR-Green I fluorescence: An alternative to the TaqMan assay for a relative quantification of gene rearrangements, gene amplifications and micro gene deletions," *BMC Biotechnol.*, vol. 3, pp. 1–13, 2003.

[33] Sigma Aldrich, "SYBR ® Green I nucleic acid gel stain," pp. 8–10, 2010.

[34] "Separation pattern." [Online]. Available: https://www.thermofisher.com/order/catalog/product/WG1601BOX.

[35] "SV40 virus." [Online]. Available: https://www.uniprot.org/uniprot/P03070.

[36] W. Denning, S. Das, S. Guo, J. Xu, J. C. Kappes, and Z. Hel, “Optimization of the transductional efficiency of lentiviral vectors: Effect of sera and polycations,” *Mol. Biotechnol.*, vol. 53, no. 3, pp. 308–314, 2013.

[37] C. Chen, S. W. Smye, M. P. Robinson, and J. A. Evans, “Membrane electroporation theories: A review,” *Medical and Biological Engineering and Computing*, vol. 44, no. 1–2. pp. 5–14, 2006.

[38] A. L. Moyer and K. R. Wagner, “Mammalian Mss51 is a Skeletal Muscle-Specific Gene Modulating Cellular Metabolism,” *J. Neuromuscul. Dis.*, vol. 2, no. 4, pp. 371–385, 2015.

[39] “KRTAP5-1.” [Online]. Available: https://www.genecards.org/cgi-bin/carddisp.pl?gene=KRTAP5-1.

[40] “FLRT1.” [Online]. Available: https://www.genecards.org/cgi-bin/carddisp.pl?gene=FLRT1.

[41] “LHFPL 4.” [Online]. Available: https://www.proteinatlas.org/ENSG00000156959-LHFPL4/tissue.

[42] “Stefin A.” [Online]. Available: http://atlasgeneticsoncology.org/Genes/GC_CSTA.html.

[43] “MYL3.” [Online]. Available: http://www.genecards.org/cgi-bin/carddisp.pl?gene=MYL3.

[44] R. Thoonen *et al.*, “Functional brown adipose tissue limits cardiomyocyte injury and adverse remodeling in catecholamine-induced cardiomyopathy,” *J. Mol. Cell. Cardiol.*, vol. 84, pp. 202–211, 2015.

[45] “H2O2 Metabolic Process.” [Online]. Available: http://software.broadinstitute.org/gsea/msigdb/cards/GO_HYDROGEN_PEROXIDE_METABOLIC_PROCESS.

[46] E. T. Chouchani, L. Kazak, and B. M. Spiegelman, “Mitochondrial reactive oxygen species and adipose tissue thermogenesis: Bridging physiology and mechanisms,” *J. Biol. Chem.*, vol. 292, no. 41, pp. 16810–16816, 2017.

[47] “Energy Homeostasis.” [Online]. Available: http://software.broadinstitute.org/gsea/msigdb/cards/GO_REGULATION_OF_ENERGY_HOMEOSTASIS.

[48] A. M. Cypess and C. R. Kahn, “The role and importance of brown adipose

tissue in energy homeostasis," *Curr. Opin. Pediatr.*, vol. 22, no. 4, pp. 478–484, 2013.

[49] Y. Nakamura and K. Nakamura, "Central regulation of brown adipose tissue thermogenesis and energy homeostasis dependent on food availability," *Pflugers Arch. Eur. J. Physiol.*, pp. 1–15, 2017.

[50] "Thyroid hormone generation." [Online]. Available: http://www.informatics.jax.org/go/term/GO:0042403.

[51] A. H. van der Spek, E. Fliers, and A. Boelen, "The classic pathways of thyroid hormone metabolism," *Mol. Cell. Endocrinol.*, vol. 458, pp. 29–38, 2017.

[52] R. Mullur, Y.-Y. Liu, and G. A. Brent, "Thyroid hormone regulation of metabolism.," *Physiol. Rev.*, vol. 94, no. 2, pp. 355–82, 2014.

[53] M.-J. Obregon, "Adipose tissues and thyroid hormones," *Front. Physiol.*, vol. 5, no. December, pp. 1–12, 2014.

[54] A. C. Bianco and E. A. McAninch, "The role of thyroid hormone and brown adipose tissue in energy homoeostasis," *Lancet Diabetes Endocrinol.*, vol. 1, no. 3, pp. 250–258, 2013.

[55] "Superoxide Metabolic Process." [Online]. Available: http://software.broadinstitute.org/gsea/msigdb/cards/GO_REGULATION_OF_SUPEROXIDE_METABOLIC_PROCESS.

[56] K. Keyer, A. Strohmeier Gort, and J. A. Imlay, "Superoxide and the Production of Oxidative DNA Damage," *J. Bacteriol.*, vol. 177, no. 23, pp. 6782–6790, 1995.

[57] R. Oelkrug, M. Kutschke, C. W. Meyer, G. Heldmaier, and M. Jastroch, "Uncoupling protein 1 decreases superoxide production in brown adipose tissue mitochondria," *J. Biol. Chem.*, vol. 285, no. 29, pp. 21961–21968, 2010.

[58] "Positive Steroid Metabolism." [Online]. Available: http://software.broadinstitute.org/gsea/msigdb/cards/GO_POSITIVE_REGULATION_OF_STEROID_METABOLIC_PROCESS.html.

[59] J. Law, I. Bloor, H. Budge, and M. E. Symonds, "The influence of sex steroids on adipose tissue growth and function," *Horm. Mol. Biol. Clin. Investig.*, vol. 19, no. 1, pp. 13–24, 2014.

[60] S. Rodriguez-Cuenca, M. Monjo, M. Frontera, M. Gianotti, A. M. Proenza, and P. Roca, “Sex steroid receptor expression profile in brown adipose tissue. Effects of hormonal status,” *Cell. Physiol. Biochem.*, vol. 20, no. 6, pp. 877–886, 2007.

[61] Z. Liu *et al.*, “Adiponectin reduces ER stress-induced apoptosis through PPARα transcriptional regulation of ATF2 in mouse adipose,” *Cell Death Dis.*, vol. 7, no. 11, p. e2487, 2016.

[62] S. Oyadomari and M. Mori, “Roles of CHOP/GADD153 in endoplasmic reticulum stress,” *Cell Death Differ.*, vol. 11, no. 4, pp. 381–389, 2004.

[63] C. Roller and D. Maddalo, “The molecular chaperone GRP78/BiP in the development of chemoresistance: Mechanism and possible treatment,” *Front. Pharmacol.*, vol. 4 FEB, no. February, pp. 1–5, 2013.

[64] S. Draghici, P. Khatri, A. C. Eklund, and Z. Szallasi, “Reliability and reproducibility issues in DNA microarray measurements,” *Trends Genet.*, vol. 22, no. 2, pp. 101–109, 2006.

[65] R. Kothapalli, S. J. Yoder, S. Mane, and T. P. Loughran, “Microarray results: how accurate are they?,” *BMC Bioinformatics*, vol. 3, p. 22, 2002.

[66] J. S. Morey, J. C. Ryan, and F. M. Van Dolah, “Microarray validation: Factors influencing correlation between oligonucleotide microarrays and real-time PCR,” *Biol. Proced. Online*, vol. 8, no. 1, pp. 175–193, 2006.

[67] A. G. Porter and R. U. Jänicke, “Emerging roles of caspase-3 in apoptosis,” *Cell Death and Differentiation*, vol. 6, no. 2. pp. 99–104, 1999.

7 List of figures and tables

8 Abbreviations

ABHD15	alpha beta hydrolase domain containing protein 15
AT	adipose tissue
ATF3	activating transcription factor 3
ATF4	activating transcription factor 4
ATGL	adipose triglyceride lipase
BAT	brown adipose tissue
BIP	binding immunoglobulin protein
BMI	body mass index (kg/m^2)
CC3	cleaved caspase 3
CD	chow diet
Cidea	cell death inducing DFFA like effector A
CHOP	transcription factor C/EBP homologous protein
DEG	differentially expressed genes
Dio 2	iodothyronine deiodinase 2
ER	endoplasmatic reticulum
FFA	free fatty acid
GSEA	gene set enrichment analysis
HGD	high glucose diet
HFD	high fat diet
H_2O_2	hydrogen peroxide
HSL	hormone sensitive lipase
iBACs	immortalized brown adipose cell line
kDa	kilo Dalton
KO	knockout
LD	lipid droplets
MGL	monoglyceride lipase
mM	milli molar
mRNA	messenger ribonucleic acid
o/e	overexpression
O_2^-	superoxide

PDE3B	phosphodiesterase 3B
pMSCV	murine stem cell virus, puro
PPAR γ	peroxisome proliferation-activated receptor γ
Pgc1α	peroxisome proliferator activated receptor gamma coactivator 1-alpha
PRDM 16	PR domain containing 16
TFIIß	transcription factor II ß
TG	triglycerides
UCP1	uncoupling protein 1
WAT	white adipose tissue
WT	wild type